



**HAL**  
open science

# Sedimentary Processes Within the Canadian Arctic Archipelago: Relationships Among Sedimentological, Geochemical, and Magnetic Sediment Properties

Sarah Letaïef, Jean-Carlos Montero-Serrano, Guillaume St-Onge

► **To cite this version:**

Sarah Letaïef, Jean-Carlos Montero-Serrano, Guillaume St-Onge. Sedimentary Processes Within the Canadian Arctic Archipelago: Relationships Among Sedimentological, Geochemical, and Magnetic Sediment Properties. *Geochemistry, Geophysics, Geosystems*, 2021, 22, 10.1029/2021GC009719 . insu-03661290

**HAL Id: insu-03661290**

**<https://insu.hal.science/insu-03661290>**

Submitted on 6 May 2022

**HAL** is a multi-disciplinary open access archive for the deposit and dissemination of scientific research documents, whether they are published or not. The documents may come from teaching and research institutions in France or abroad, or from public or private research centers.

L'archive ouverte pluridisciplinaire **HAL**, est destinée au dépôt et à la diffusion de documents scientifiques de niveau recherche, publiés ou non, émanant des établissements d'enseignement et de recherche français ou étrangers, des laboratoires publics ou privés.

Copyright

# Geochemistry, Geophysics, Geosystems

## RESEARCH ARTICLE

10.1029/2021GC009719

### Key Points:

- Sedimentological, geochemical and magnetic baseline data are reported in the Canadian Arctic Archipelago
- Sedimentary processes that operate within Canadian Arctic Archipelago during the pre- and post-industrial periods are documented
- Regional <sup>210</sup>Pb-dated box cores provide clues about the sedimentary dynamics that operated during the Little Ice Age

### Supporting Information:

Supporting Information may be found in the online version of this article.

### Correspondence to:

S. Letaïef,  
[Letaief-Sarah@laposte.net](mailto:Letaief-Sarah@laposte.net)



### Citation:

Letaïef, S., Montero-Serrano, J.-C., & St-Onge, G. (2021). Sedimentary processes within the Canadian Arctic Archipelago: Relationships among sedimentological, geochemical, and magnetic sediment properties. *Geochemistry, Geophysics, Geosystems*, 22, e2021GC009719. <https://doi.org/10.1029/2021GC009719>

Received 22 FEB 2021

Accepted 17 JUN 2021

## Sedimentary Processes Within the Canadian Arctic Archipelago: Relationships Among Sedimentological, Geochemical, and Magnetic Sediment Properties

Sarah Letaïef<sup>1</sup> , Jean-Carlos Montero-Serrano<sup>2,3</sup> , and Guillaume St-Onge<sup>2,3</sup>

<sup>1</sup>Géosciences Montpellier, Université de Montpellier, CNRS, Montpellier, France, <sup>2</sup>Institut des sciences de la mer de Rimouski, Université du Québec à Rimouski, Rimouski, QC, Canada, <sup>3</sup>GEOTOP Research Center, Montréal, QC, Canada

**Abstract** The sedimentological, geochemical, physical and magnetic properties of 40 surface and basal sediment samples of box cores collected throughout the Canadian Arctic Archipelago (CAA) from the Canadian Beaufort Shelf to Lancaster Sound were analyzed to determine the sedimentary processes that operate within the CAA during the pre- and post-industrial periods (i.e., before and after 1900 Common Era or CE). In addition, the chronology of seven selected regional cores was established using <sup>210</sup>Pb measurements, where the base is dated between 1550 and 1820 CE. These cores provide an opportunity to robustly compare post-1900 sedimentary conditions with those of the colder Little Ice Age period (LIA; ~1500–1900 CE). The different properties combined with multivariate statistical analyses result in the identification of three regional provinces with distinct sedimentary characteristics: (a) the West province (Mackenzie Shelf/Slope, west Banks Island and M'Clure Strait) typified by detrital associations (Fe-Rb-Ti-Zn), high organic matter inputs, dominance of magnetite and low-coercivity minerals and high aluminosilicate contents; (b) the Intermediate Zone (Amundsen and Coronation gulfs) distinguished by Si-Al-Zr-Sr-K associations, Mn oxyhydroxides precipitation, constant high magnetic grain concentrations and a mixture between marine and terrigenous organic matter; and (c) the East Province (Queen Maud Gulf, Victoria and Barrow straits, and Lancaster and Eclipse sounds) described by high detrital carbonate inputs, marine organic matter, a dominance of high-coercivity minerals and high magnetic concentrations in pre-industrial samples. Our results confirm that the pre- and post-industrial sedimentary dynamics are controlled by sediment supplies from the river discharges in the West and Intermediate provinces, whereas the East province is more influenced by sea ice and coastal erosion. Basal sediment samples from the seven <sup>210</sup>Pb-dated cores suggest an intensification of the Mackenzie, Coppermine, and Ellice rivers runoff, extensive sea-ice cover and consequently sediment transport by the latter during the LIA period.

**Plain Language Summary** The Arctic is a region where the seafloor composition is the least studied and understood. Indeed, the vast majority of the channels within the Canadian Arctic Archipelago (CAA) and their adjoining continental shelves and slopes exhibit a substantial knowledge gap regarding sediment composition. This information is essential to provide fundamental baseline data on the physical and chemical sediment properties as well as to determinate fingerprints for sediment source areas and sediment transport processes in this Arctic region. In this regard, the present study is interested in the sedimentary processes regional heterogeneity that operate within the CAA during the pre- and post-industrial periods, which was investigated through magnetic, geochemical and sedimentological analyses of 40 surface and 40 basal sediments retrieved from the Canadian Beaufort Shelf to Lancaster Sound. Pre- and post-industrial sedimentary processes are mainly influenced by river discharge in the west and central CAA, and by coastal erosion and sediment-laden sea ice in the east CAA. The results obtained here provide a basis for future studies using the sedimentological, geochemical and magnetic signatures of longer sediment records from the CAA to reconstruct variations in sediment dynamics related to late Quaternary climatic and oceanographic changes.

## 1. Introduction

Polar regions act as the world's thermostat by providing a strong albedo with their perennial or seasonal sea-ice cover. During the past decades, the Arctic seems to be the most global region affected by climate warming, with a decrease of 12.4% per decade in summer sea-ice extent (Comiso et al., 2017; Stroeve et al., 2011) accompanied by a loss of ice older than 5 years. Recently, less than 5% of the Arctic Ocean ice observed is older than 5 years, compared to 20% in the 1980s (Serreze & Stroeve, 2015), responding to the increase in greenhouse gas emissions (Pachauri et al., 2014). The rapid loss of sea-ice cover and thereby the reduced albedo has played a role in amplifying Arctic warming (Cohen et al., 2014; Holland & Bitz, 2003; Serreze & Francis, 2006; Serreze et al., 2008). The magnitude of these changes around the Arctic shows regional patterns and generally results in an increase in temperature and precipitation due to enhanced evaporation (Bintanja & Selten, 2014; Kopec et al., 2016), northward transport of moisture (Zhang et al., 2013) and intensification of the hydrological cycle (Huntington, 2006; Peterson et al., 2006), depending on the region.

During the last decade, paleoclimatic studies have become more frequent for the Arctic region (Fennoscandia, Arctic Canada, Alaska and Greenland) using numerous proxies from natural archives such as lakes (Gajewski, 2002, 2006, 2015), peat (Ruppel et al., 2013; Zhang et al., 2017), marine sediments (e.g., Bringué & Rochon, 2012; Caron et al., 2019, 2020; Deschamps, Montero-serrano, et al., 2018; Deschamps, St-Onge, et al., 2018; Durantou et al., 2012; Ledu, Rochan, de Vernal, Barletta, & St-Onge, 2010; Ledu, Rochon, de Vernl, & St-Onge, 2010; Pieńkowski et al., 2011, 2013; Stokes et al., 2005; among others), ice cores (Mosley-Thompson et al., 2001; Paterson & Waddington, 1984) and tree rings (Helama & Lindholm, 2003; Linderholm & Chen, 2005; Pisaric et al., 2009). A recent review summarizes Arctic hydroclimate changes during the last two millennia (Linderholm et al., 2018), where hydroclimate simulations and proxies generally reveal that the Little Ice Age (LIA, 1500–1900 Common Era or CE; Jones & Mann, 2004) was drier (Ljungqvist et al., 2016) even if large regional differences are observed. During the last 2000 years, an increase in precipitation (Viau & Gajewski, 2009) and river runoff (Wagner et al., 2011) and general colder reconstructed summer sea surface temperatures in the Mackenzie Delta (e.g., Bringué & Rochon, 2012) have been shown in the western Canadian Arctic Archipelago (CAA), whereas a decrease in precipitation (Viau & Gajewski, 2009), an increase in sea-ice cover and colder conditions have been described in the southwest (Pieńkowski et al., 2011, 2017) and central CAA (e.g., Belt et al., 2010; Vare et al., 2009).

Comparisons between different Arctic areas allow the reconstruction of the climatic mosaic and the Arctic response to ongoing global warming, but the lack of spatiotemporal analyses makes comparisons difficult. Since the CAA constitutes a large area controlled by several sedimentary processes, the aims of this work are to reconstruct and compare sedimentary processes during the pre- and post-industrial periods (i.e., before and after 1900 Common Era or CE) as well as during the LIA within this Arctic region. To achieve these objectives, we use sedimentological, magnetic and geochemical proxies from box cores covering a large part of the CAA in order to compare the sediment properties from (a) the surface (post-1900) and basal (pre-1900) sediment samples of the cores and (b) the LIA interval of seven  $^{210}\text{Pb}$ -dated box cores.

### 1.1. Regional Settings

#### 1.1.1. Regional Characteristics and Hydrology

The CAA is a complex array of Islands covering an area of 2.9 million  $\text{km}^2$  that represents  $\sim 20\%$  of the total shelf area in the Arctic (Jakobsson, 2002). Narrow channels formed by glacial erosion during the Quaternary (England et al., 2006) is interconnected with larger basins. Furthermore, the Northwest Passage connects the eastern (Baffin Bay) and western (Beaufort Sea) Canadian Arctic through the CAA and represents one of the three main routes connecting on a larger scale the Arctic Ocean to the Labrador Sea and North Atlantic. For this reason, the CAA is considered to be a key area for mass and heat exchanges between the Arctic and Atlantic Oceans (Dickson et al., 2007; Melling, 2002; Melling et al., 2001; Michel et al., 2006). The export of water through Nares and Fram straits and the Northwest Passage influence the formation of Atlantic deep waters (Aagaard & Carmack, 1989, 1994) and thereby impact the global thermohaline circulation (Proshutinsky et al., 2002). Because of the large freshwater inputs (including river discharges, summer sea-ice melting and precipitation), the Arctic water column is strongly stratified, creating advection from the relatively fresh upper layer (Aagaard & Carmack, 1989). Typically, a cold and low-salinity surface

layer named the Polar Mixed Layer (PML) is found in the upper 50–100 m depths and is mainly formed by summer meltwaters and river discharges. From depths of 100–300 m the PML is underlain by warmer and low-salinity Pacific waters added to a contribution from Mackenzie and Yukon river waters via the Alaska Coastal Current (Jones et al., 2003). Finally, a strong halocline separates the Pacific waters from the Atlantic waters until depths of 500–800 m which enters into the system through the west Spitsbergen and west Greenland currents (Woodgate et al., 2007).

Furthermore, the highly complex inter-island dynamics in the archipelago are mainly explained by the presence of shallow channels: in the West, water depths reach ~550 m except close to M'Clure Strait, where a sill causes a decrease in water depth of ~375 m. In the East, the limiting sill is in Barrow Strait, where the depth is ~125 m and increases gradually eastward to ~500 m in Lancaster Sound and then to over 2,000 m in Baffin Bay (McLaughlin et al., 2004). Consequently, the water column is predominantly composed of Pacific waters (Jones et al., 2003) that originate from the Canadian Basin via the M'Clure Strait and the Amundsen Gulf. In the western part, the general water mass circulation (Figure 1a) in the CAA is strongly influenced by the anticyclonic Beaufort Gyre (BG), whereas the central CAA is driven by a net southeastward circulation (Ingram & Prinsenberg, 1998).

### 1.2. Climate and Sea Ice

In the CAA, the meteorology variable both regionally and temporally (McLaughlin et al., 2004). During winter, recent mean air temperatures are close to  $-30^{\circ}\text{C}$ , whereas the cool summers are characterized by mean temperatures of  $4^{\circ}\text{C}$ . In the western part of the CAA, recent meteorological conditions are driven by the fluctuations in the large-scale Arctic Oscillation (Barber & Hanesiak, 2004). In the West, the semipermanent high-pressure system located over the Beaufort Sea during winter impacts the regional climate (Agnew & Silas, 1995), whereas in the East, the local climate is affected by wind forcing and specific topography (Ingram & Prinsenberg, 1989). Presently, the CAA is covered by sea ice annually with a strong seasonality. The formation of sea ice begins mid-September, and sea ice starts to break up in late May, while the minimum sea-ice cover is observed late August (Canadian Ice Service, 2019).

Paleoreconstructions in the Northern Hemisphere show a general decrease in summer temperatures over the past 8 cal ka BP, reflecting the continuous insolation decrease resulting from the precession of the equinoxes (Wanner et al., 2011). The changes in summer temperatures have been more significant in the Arctic than in other places (Kaufman et al., 2004; Vinther et al., 2009) and were established after medieval times. In addition, anomalously cold summers at century-scale intervals have been recorded by most glaciers and ice caps from the CAA, related to the colder LIA period (Jones & Mann, 2004). Notwithstanding the variety of records defining climate change during the past millennium (Mann et al., 2008), there is no clear consensus about the timing and duration and what factors contributed to generating and maintaining LIA conditions. Globally, this cold time period within the CAA is included between 1500 and 1900 CE (Bradley & Jones, 1993; Jones & Mann, 2004) but also differ regionally: between 1500 and 1900 CE in Mackenzie Shelf/Slope (Bringué & Rochon, 2012; Durantou et al., 2012; Richerol et al., 2008); ~1680–1940 CE in Coronation Gulf (Pieńkowski et al., 2011; 2017); ~1500–1900 CE in Victoria Strait (Belt et al., 2010); 1650–1900 CE in Lancaster Sound/Baffin Bay (Ledu, Rochon, de Vernal, Barletta, & St-Onge, 2010; Ledu, Rochon, de Vernal, & St-Onge, 2010); and ~1550–1850 CE in Devon Ice Cap/Ellesmere (Koerner, 1977; Koerner & Fisher, 1990; Koerner & Paterson, 1974).

### 1.3. Surrounding Geology

The Mackenzie River drains a basin of  $1.78 \times 10^6 \text{ km}^2$  (Aziz & Burn, 2006; Hill et al., 2001). The basin is characterized in the western part by the North American Cordillera geological unit (Mackenzie and Rocky Mountain belts; Millot et al., 2003) composed of sedimentary and volcanic rocks (Figure 1b) and in the eastern part by the Canadian Shield in the Slave Province, which comprises Archean granites and gneisses (Millot et al., 2003). In turn, Banks Island is mostly composed of Cretaceous to upper Paleozoic sedimentary rocks (Figure 1b) and Quaternary dolomite-rich tills (Bischof & Darby, 2000; Bischof et al., 1996). Otherwise, most of the Islands such as Victoria and Prince of Wales Islands, are typically underlain by Ordovician and Silurian detrital carbonates (Figure 1b; Stokes et al., 2009). Finally, eastern Lancaster Sound is

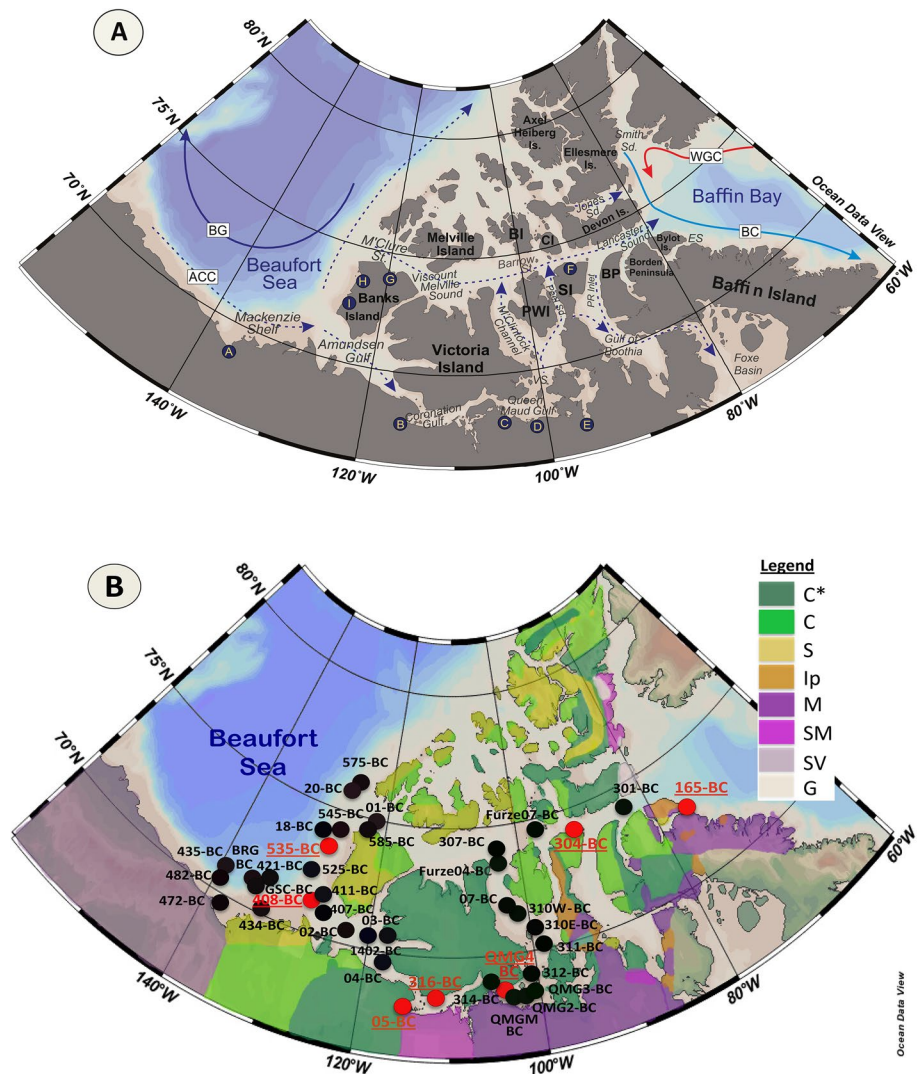


**Figure 1.** (a) Map of the Canadian Arctic Archipelago (CAA) showing geographical locations mentioned in the text and the generalized surface water circulation (dashed arrows) based on Ingram and Prinsenber (1998) and Michel et al. (2006). Some important rivers are also identified (blue circle): A, Mackenzie River; B, Coppermine River; C, Ellice River; D, Simpson River; E, Back and Hayes rivers, F, Cunningham River; G, Thomsen River; H, Bernard River, and I = Big River. BG, Beaufort Gyre; ACC, Alaskan Coastal Current; BC, Baffin Current; WGC, West Greenland Current; VS, Victoria Strait; VWI, Prince of Wales Island; SI, Somerset Island; BI, Bathurst Island; CI, Cornwallis Island; PR Inlet, Prince Regent Inlet; Peel Sd., Peel Sound; BP, Brodeur Peninsula; ES, Eclipse Sound; Jones Sd., Jones Sound. (b) Map of the geological setting illustrating the location of surface and core sediment samples used in this study. The red colored stations correspond to  $^{210}\text{Pb}$  dated cores. Simplified geological units map of the CAA based on studies from Wheeler et al. (1996), Harrison et al. (2011) and Alkire et al. (2017). The color code represents the dominant facies: C\*, dominant carbonate/evaporite; C, major carbonate unit; S, sedimentary facies; Ip, plutonic; M, metamorphic; SM, sedimentary and metamorphic, SV, sedimentary and volcanic; G, unknown deposit influenced by the ancient glacier coverage.

defined by Cretaceous to Plio-Pleistocene geological units associated with rifting (Li et al., 2011; MacLean et al., 1990) and Bylot Island is characterized by plutonic igneous rocks belonging to the Canadian Shield (Wheeler et al., 1996).

#### 1.4. Sediment Dynamics

The mean annual discharge of the CAA rivers was recently estimated to be  $\sim 202 \text{ km}^3/\text{yr}$  (Alkire et al., 2017; Lammers et al., 2001). Although the Mackenzie River discharge in the system is significant ( $\sim 420 \text{ km}^3/\text{yr}$ ;

Wagner et al., 2011), many CAA small rivers exist, including the Coppermine River ( $\sim 88 \text{ km}^3/\text{yr}$ ), Ellice and Back rivers ( $\sim 2.82 \text{ km}^3/\text{yr}$  and  $\sim 15.52 \text{ km}^3/\text{yr}$  respectively; Déry, 2016) and the Cunningham River ( $\sim 3.28 \text{ km}^3/\text{yr}$ ). Their cumulative discharge is large enough to significantly impact the freshwater flowing through the CAA and the local sedimentation.

The most important sediment entrainment in the Beaufort Sea, the Northwest Passage and globally in the Arctic Ocean is a suspension freezing by frazil and anchor ice (Darby et al., 2011; Reimnitz et al., 1993). During rapid ice formation in open and shallow water areas, frazil incorporates fine-grained suspended sediment that is disseminated along its way (Reimnitz & Barnes, 1987; Reimnitz et al., 1993). Indeed, fine-grained sediments discharged from coastal erosion or river drainages within the first 25–30 m water depth are disseminated into the first-year ice during freezing storms. Then they are transported by ice until the ice motion is stopped for the duration of winter and finally deposited elsewhere during rapid summer melting (Reimnitz et al., 1993). By using Fe-oxide fingerprinting grains, Darby (2003) showed that western Canadian Arctic sea-ice floes drift west from the Laptev Sea to Beaufort Gyre via the Transpolar Drift. Aeolian transport in the CAA has been identified as insignificant and very localized (Darby et al., 1974; Reimnitz & Maurer, 1979). In the context of current climate change, sea ice becomes more seasonal, and coasts have enhanced permafrost. Consequently, un lithified ice-bonded coasts in the West area and high cliffs in the East promote conditions for coastal erosion (Overduin et al., 2014). For instance, the prograded beach morphology on Cape Charles Yorke (Baffin Bay) is an excellent case that shows a recent shift in sedimentary processes from deposition to erosion, resulting from a lower sediment supply, increased wave energy and sea level rise (St-Hilaire-Gravel et al., 2011).

## 2. Materials and Methods

### 2.1. Coring and Sampling

In total, 40 box cores were collected at various depths in eight different regions (Figure 1b), including the Mackenzie Shelf/Slope, the Amundsen Gulf, the M'Clure Strait, Coronation and Queen Maud gulfs, the M'Clintock Channel, the Barrow Strait, and the Eclipse Sound on board of the Canadian Coast Guard Ship (CCGS) Amundsen as part of the ArcticNet program in 2016 (Montero-Serrano et al., 2016; Table 1). All coring sites were targeted using high-resolution seismic profiles that indicated high sediment accumulation not influenced by mass wasting events (Montero-Serrano et al., 2016). In each box core, two push cores were subsampled. Using the results from digital X-ray and continuous multi-sensor core logger (MSCL) measurements processed in the lab, one replicate push core was selected for subsequent analyses based on the absence of coring disturbance/artifacts and the absence of compaction visually confirmed on deck during the sampling. To study the sediment-water interface, surface sediment samples were collected on board in the uppermost 1 cm of each box core using a spatula and stored in plastic bags. Furthermore, once split, the cores were sampled with  $1 \text{ cm}^3$  cubes at the top (representing the first 1 cm) and the base (the lowest centimeter in each core; Table 1). Overall, a total of 40 surface and 40 basal sediment samples were used for discrete grain size, magnetic and sedimentological analyses.

### 2.2. Continuous Physical and Geochemical Analyses

All the box cores were opened, described, photographed and analyzed with the GEOTEK MSCL in split core mode at 0.5 cm intervals. With this setting, the following parameters were determined: diffuse spectral reflectance ( $L^*$  and  $a^*$ ) using a Konica Minolta CM2600d spectrophotometer, low-frequency magnetic susceptibility ( $k_{LF}$ ) using a point source sensor and chemical composition (Ti, Mn, Fe, Al, Si, K, Ca, Zn, Rb, Sr, and Zr) using a portable Olympus Delta Professional X-ray fluorescence (pXRF) sensor. The pXRF data enabled the calculation of geochemical ratios in order to derive more information about sedimentological processes, such as the  $\text{Log}(\text{Al}/\text{Ca})$  and  $\text{Log}(\text{Mn}/\text{Al})$  ratios, which have previously been used to reconstruct changes in sediment provenance and transport (Croudace & Rothwell, 2015; Croudace et al., 2006).  $\text{Log}(\text{Al}/\text{Ca})$  provides a straightforward proxy to reflect sediment sources where the Al can be associated with aluminosilicate inputs (Nizou et al., 2011) and Ca with detrital carbonates. Given that Mn is a highly insoluble oxyhydroxide when oxic conditions prevail (Burdige, 1993; Calvert & Pedersen, 2007), enrichment in Mn

**Table 1**  
*Coordinates and Depths for the Studied Sediment Cores*

Official labels of sample stations	Labels used in this study	Latitude (°N)	Longitude (°W)	Depth (m)	Basal depth (cm)	Regional location
AMD16-Lakeman-08-01-BC	01-BC	74.8855	122.17016	505	40	M'Clure Strait
AMD16-0416-02-BC	02-BC	70.6085	123.0285	628	39.5	Amundsen Gulf
AMD16-0416-03-BC	03-BC	70.5138	120.34866	330	41.5	Amundsen Gulf
AMD16-0416-04-BC	04-BC	69.8645	117.85616	415	42.5	Amundsen Gulf
AMD16-0416-05-BC	05-BC	67.8645	115.07168	60	36.5	Coronation Gulf
AMD16-07-BC	07-BC	71.8692	102.7247	245	39.5	Victoria Strait
AMD16-1402-BC	1402-BC	70.5463	117.6323	400	40	Amundsen Gulf
AMD16-165-BC	165-BC	72.7092	75.761166	645	42.5	Eclipse Sound
AMD16-Lakeman-07-2016-805-18-BC	18-BC	74.0076	129.127	420	44.5	West Banks Island
AMD16-2016-805-20-BC	20-BC	75.7415	126.47666	373	27	M'Clure Strait
AMD16-301-BC	301-BC	74.1211	83.31972	740	38	Lancaster Sound
AMD16-304-BC	304-BC	74.2462	91.521966	314	45	Lancaster Sound
AMD16-307-BC	307-BC	74.1022	103.01421	350	37.5	Barrow Strait
AMD16-310E-BC	310E-BC	70.8324	99.076616	216	42	Victoria Strait
AMD16-310W-BC	310W-BC	71.4594	101.2724	163	23	Victoria Strait
AMD16-311-BC	311-BC	70.2809	98.5341	170	42	Victoria Strait
AMD16-312-BC	312-BC	69.1668	100.69713	66	45	Queen Maud Gulf
AMD16-314-BC	314-BC	68.9718	105.47513	89	35	Queen Maud Gulf
AMD16-316-BC	316-BC	68.389	112.092	182	40	Coronation Gulf
AMD16-407-BC	407-BC	71.01	126.09	390	45	Amundsen Gulf
AMD16-408-BC	408-BC	71.3038	127.57483	205	41	Amundsen Gulf
AMD16-411-BC	411-BC	71.6236	126.731	435	42.5	Amundsen Gulf
AMD16-421-BC	421-BC	71.3998	133.89066	1135	42	Mackenzie Slope
AMD16-434-BC	434-BC	70.174	133.54416	46	49	Mackenzie Shelf
AMD16-435-BC	435-BC	71.0768	139.6579	290	38.5	Mackenzie Slope
AMD16-472-BC	472-BC	69.612	138.227	124	40	Mackenzie Shelf
AMD16-482-BC	482-BC	70.5245	139.385	821	43	Mackenzie Shelf
AMD16-525-BC	525-BC	72.3924	128.95231	347	40	West Banks Island
AMD16-525-BC	535-BC	73.4163	128.192	289	21	West Banks Island
AMD16-525-BC	545-BC	74.1784	126.82341	315	39	West Banks Island
AMD16-525-BC	575-BC	76.1555	125.87401	318	22	M'Clure Strait
AMD16-525-BC	585-BC	74.5131	123.22216	382	37.5	M'Clure Strait
AMD16-BRG-BC	BRG-BC	70.9923	135.46266	664	37	Mackenzie Shelf
AMD16-FURZE04-BC	Furze4-BC	73.6487	103.38916	245	31.5	Victoria Strait
AMD16-FURZE07-BC	Furze7-BC	74.7068	97.19565	318	44	Barrow Strait
AMD16-GSCLander2-BC	GSC-BC	70.8756	135.00083	200	38	Mackenzie Shelf
AMD16-QMG2-BC	QMG2-BC	68.3164	100.80323	53	36	Queen Maud Gulf
AMD16-QMG3-BC	QMG3-BC	68.3141	102.94483	56	40	Queen Maud Gulf
AMD16-QMG4-BC	QMG4-BC	68.4901	103.41886	82	45	Queen Maud Gulf
AMD16-QMGM-BC	QMGM-BC	68.3103	101.76546	107	41	Queen Maud Gulf

is associated with oxic conditions. Finally,  $\text{Log}(\text{Mn}/\text{Al})$  is used as an indicator of bottom water ventilation (Gamboa et al., 2017).

### 2.3. Carbon and Nitrogen Analyses

Carbon and nitrogen analyses were performed for surface and basal sediments in order to determine the spatial variations in the sedimentary organic matter sources (terrestrial vs. marine) and inorganic carbon ( $C_{\text{inorg}}$ ) content (e.g., Meyers, 1994; St-Onge & Hilaire-Marcel, 2001). The first aliquot of 6–10 mg of bulk sediment was dried, homogenized and encapsulated for total carbon ( $\%C_{\text{tot}}$ ) and total nitrogen ( $\%N_{\text{tot}}$ ) contents. A second aliquot of 8–12 mg of sediments was acidified with 0.2 ml HCl (1 M) to dissolve carbonates in order to measure organic carbon ( $\%C_{\text{org}}$ ) contents. Both aliquots were analyzed using the CF-IRMS (continuous flow isotope ratio mass spectrometry) coupled with a COSTECH 4010 (Costech Analytical) elemental analyzer. The  $\delta^{13}\text{C}_{\text{org}}$  content was analyzed in the acidified aliquot portion, whereas the  $\delta^{15}\text{N}_{\text{tot}}$  content was measured using the bulk samples with a gas chromatograph coupled to a ThermoScientific Deltaplus XP mass spectrometer where the analytical errors ( $n=50$ ) of measurement were 0.2 and 0.4‰, respectively. System suitability prior to analysis was evaluated using standards (caffeine, nannochloropsis and Mueller Hinton Broth). The  $C_{\text{inorg}}$  content was calculated by subtracting  $C_{\text{org}}$  from  $C_{\text{tot}}$  content. The  $C_{\text{org}}/N_{\text{tot}}$  ratio is expressed as an atomic C/N ratio and used to distinguish between marine and terrestrial sources for sedimentary organic matter (OM; Meyers, 1994; 1997).

### 2.4. Grain Size Measurements

Approximately 1 g of sediment was moistened with  $\text{H}_2\text{O}$ . Afterward, 10 ml of hydrochloric acid (1 M HCl) and hydrogen peroxide (30%  $\text{H}_2\text{O}_2$ ) was added to remove biogenic carbonates and organic material, respectively, in order to isolate the detrital fraction. Samples were then deflocculated by successive washing with distilled water and analyzed with a Beckman Coulter LS13320 laser diffraction grain-size analyzer, which had a detection range of 0.04–2000  $\mu\text{m}$ . The statistical parameters (e.g., sorting and mean grain size) were computed with the GRADISTAT software (Blott & Pye, 2001) by using the method of moments on the logarithmic phi-scale.

### 2.5. Discrete Magnetic Analyses

The sampled cubes were analyzed with a 2G SRM-755 cryogenic magnetometer. Isothermal remanent magnetization and saturated isothermal magnetization (IRM and SIRM, respectively) were acquired using a 2G-pulse magnetizer in DC fields of 300 and 950 mT. IRM was then demagnetized at a peak alternating field (AF) of 0–80 mT at 5 mT steps. In the case of SIRM, the demagnetization steps were operated at 0, 5, 10, 30, 50, and 80 mT. By dividing the IRM imparted at 300 mT by the SIRM (950 mT), we calculated the pseudo S-ratio in order to estimate the magnetic mineralogy. Values close to 1 indicate the presence of lower-coercivity ferrimagnetic minerals (e.g., magnetite), whereas lower values indicate the contribution from higher-coercivity minerals (e.g., hematite). The median destructive field (MDF) is the required field to remove half of the initial remanence and is influenced by magnetic grain size and mineralogy. In this paper, we use the  $\text{MDF}_{\text{IRM}}$  to obtain information on the coercivity of the magnetic mineral assemblages.

For surface and basal samples, magnetic susceptibility was measured using a Bartington MS2E instrument. To determine the frequency dependence, magnetic susceptibility measurements were performed in a magnetic field created by two frequencies: a low frequency at 0.46 Hz and a high frequency at 4.6 Hz. The difference between these two measurements was used to detect the presence of superparamagnetic minerals (e.g., Dearing, 1999) characterized by slightly lower susceptibility values at high frequency. Ultrafine superparamagnetic crystals are smaller than  $\sim 0.03 \mu\text{m}$  and show rapid changes over time in their magnetic behavior (Dearing, 1999).

Finally, samples were measured using a Princeton Measurement Corporation alternating gradient force magnetometer (MicroMag 2900 AGM) to determine the coercivity force ( $H_c$ ), the coercivity of remanence ( $H_{cr}$ ), the saturation magnetization ( $M_s$ ) and the saturation remanence ( $M_{rs}$ ). The resulting coercivity



( $H_{cr}/H_c$ ) and remanence ( $M_{rs}/M_s$ ) ratios and the shape of the hysteresis loops are indicative of the magnetic mineralogy and grain size (Day et al., 1977; Dunlop, 2002).

## 2.6. Sediment Dating

Recent sedimentation rates were calculated from seven cores representative of each part of the study area (05-BC, 165-BC, 304-BC, 316-BC, 408-BC, 535-BC, and QMG4-BC) and based on  $^{210}\text{Pb}$  measurements at GEOTOP (Montréal). Approximately 2 g of dried and crushed sediment was sampled at 1 cm intervals until 15 cm and at every 5 cm thereafter until reaching the core bottom. The  $^{210}\text{Pb}$  measurements were made after chemical treatment purification and deposition on a silver disk following routine procedures and using an EGG ORTEC model 576 alpha spectrometer (Hamilton & Smith, 1986). Excess  $^{210}\text{Pb}$  measurements were processed by counting the activity of the  $^{210}\text{Po}$  daughter isotope (Appleby & Oldfield, 1984; Zhang, 2000), and  $^{209}\text{Po}$  was used as the chemical yield. The counting error was evaluated at  $1\sigma \sim 2\text{--}4\%$ . To estimate the sedimentation rates, we first visually determined  $^{210}\text{Pb}_{\text{supported}}$  and second calculated  $^{210}\text{Pb}_{\text{excess}}$  ( $^{210}\text{Pb}_{\text{excess}} = ^{210}\text{Pb} - ^{210}\text{Pb}_{\text{supported}}$ ). Then, the CRS model (constant rate of  $^{210}\text{Pb}$  supply; Appleby & Oldfield, 1983; Oldfield & Appleby, 1984), the slope of the linear regression  $\ln(^{210}\text{Pb}_{\text{ex}})$  and depth was used to calculate the average sedimentation rate ( $\text{SR}) = -\ln(2)/(\text{slope} * 22.3)$ , where 22.3 is the half-life of  $^{210}\text{Pb}$  (e.g., Ghaleb, 2009). This SR allowed us to estimate the age of the base of the measured cores.

Furthermore, we used the magnetic susceptibility variations measured along the cores to link the dated cores with the nearby undated ones for each region (Figures S1–S4). Prominent magnetic susceptibility features identified in the upper parts of the cores (post-1900 interval) from the same regions allowed to correlate. Likewise, most of the magnetic susceptibility profiles from each region show a uniform shape in the bottom parts of the cores (pre-1900 interval). No major magnetic susceptibility variations or sudden amplitude changes are observed at the base of the cores in each region that would suggest different environmental conditions, and therefore, substantially different time periods. In addition, sedimentation rates (cm/ka) data available within the CAA were compiled in an interpolated map (Figure S5). Based on all this information, we assumed that surface sediments accumulated after 1900 CE, whereas basal sediments most likely accumulated prior to 1900 CE.

## 2.7. Statistical and Spatial Approach

Due to its large regional climatic and oceanographic variability, sedimentary processes operating across the CAA referenced in paleoenvironmental studies and actual descriptions vary from region to region. Indeed, this variability has been notably explained by the influence of the Mackenzie River and the small Canadian Arctic rivers in the western part of the CAA (Alkire et al., 2017; Belt et al., 2010; Bringué & Rochon, 2012; Durantou et al., 2012; Gamboa et al., 2017; Scott et al., 2009; Wagner et al., 2011) and the influence of sea ice in the eastern part of the study area (Ledu, Rochon, de Vernal, Barletta, & St-Onge, 2010; Ledu, Rochon, de Vernal, & St-Onge, 2010; Pieńkowski et al., 2011, 2013). Considering the vastness of the study area, sedimentary provinces characterized by their own processes were statistically defined using cluster analysis. Therefore, sampling sites were arranged in a hierarchical cluster using the major surface geochemical elements (Ti-Mn-Fe-Al-Si-K-Ca) from the pXRF data set in order to identify different sedimentological provinces. In addition, to gain information on the degree of mixing between the clusters, a fuzzy c-means (FCM) clustering analysis was also performed using the pXRF major elements data. The results from the FCM clustering are visualized in a silhouette plot (Kassambara, 2017). The silhouette plot allows visualization of the robustness of clusters (Borcard et al., 2011), where each sample is represented by a bar (silhouette width) that ranges from 0 (no similarity) to 1 (identical). Both hierarchical and FCM analysis were performed using the Aitchison distance between the samples as a measure of dissimilarity and Ward's method for agglomerative calculation purposes. To obtain a statistical link among several variables by detecting elemental associations with similar relative variation patterns that may be interpreted from a paleoenvironmental standpoint (e.g., Gamboa et al., 2017; Montero-Serrano et al., 2010; von Eynatten et al., 2003, 2016), principal component analysis (PCA) was performed on the pXRF data from surface and basal samples. Note that Mn was not used in the PCA, since it has a large influence on the total variance of the pXRF data set. The non-parametric Spearman rank method was used to measure the correlation between diffuse spectral reflectance ( $L^*$  and  $a^*$ ), pXRF and carbon data, and the results were visualized in a correlation matrix.

Statistical analyses were conducted with R software (R Core Team, 2021) using the packages “compositions” (van den Boogaart & Tolosana-Delgado, 2008, 2021), “factoextra” (Kassambara & Mundt, 2020), “cluster” (Maechler et al., 2019), and “ggcorrplot” (Kassambara, 2016).

The geochemical data are compositional, that is, vectors of nonnegative values subjected to a constant-sum constraint (of 100%). This feature implies that relevant information is usually contained in the relative magnitudes and that the statistical analysis must focus on the ratios between components (Aitchison, 1986). Prior to multivariate analysis, a log-centered (clr) transform is applied (Aitchison, 1990). This transformation first divides the elemental concentration by the geometric mean of the compositions of the individual observations and then uses the logarithm. Note that all the geochemical element ratios are expressed as log-ratios in order to minimize the highest values and distribute the lowest one, which is most suitable for right-skewed distributions (van den Boogaart & Tolosana-Delgado, 2013).

Finally, physical and magnetic properties, grain size and carbon-nitrogen data, as well as the score from the first principal component (PC1) of the log-centered pXRF data, are used to produce interpolated maps using the Ocean Data View (ODV) software (Schlitzer, 2018). The interpolated maps are generated using a weighted-average gridding algorithm with a quality limit of 1.2.

### 3. Results

#### 3.1. Sedimentological and Physical Properties

##### 3.1.1. Spatial Delimitation Based on Elemental Geochemistry

Hierarchical and FCM analysis reveal similar results and indicate that there are three geographical clusters within the CAA with distinct geochemical compositions (Figures 2a–2c). Cluster 1 is mainly represented by samples from the western CAA (M’Clure Strait, west Banks Island, the Mackenzie Shelf/Slope) and also by samples from the mouth of Coppermine and Ellice rivers. Cluster 2 is represented by samples mainly originating from the Amundsen Gulf, with some samples from the west Banks Island and Coronation and Queen Maud gulfs (this cluster is hereafter referred as Intermediate Zone or IZ). Cluster 3 is mostly represented by samples from the eastern CAA (Queen Maud Gulf, Victoria and Barrow straits, and Lancaster and Eclipse sounds). The silhouette plot reveals that 100% of the sediment samples are correctly classified (Figure 2b). However, most of samples with below-average silhouette width values (<0.29) are samples from cluster 1 (West province), likely due to a greater mix of different sediment sources. PCA of pXRF data reveal two PC scores which explain 71.5% of the total variance (54.4% and 17.1% for PC1 and PC2 scores, respectively; Figure 2d). PC1-scores are positively associated with Ti-Fe-Rb-Zn and negatively associated with Ca. PC2-scores shows anti-correlation between Sr-Zr and Al-Si. It is also important to mention that Mn is removed from the PCA because of its strong influence on geochemical variability. The spatial distributions of the PC1-scores for surface and basal sediments depict large positive PC-1 scores (Ti-Fe-Rb-Zn) in most of the West province stations and large negative PC-1 scores (Ca-Si) in the East province stations (Figures 3a and 3b). Intermediate PC-1 scores (Al-Si-Sr-Zr) are observed in most of the IZ stations.

The Log(Mn/Al) distribution map shows higher concentrations for surface sediments especially south of Banks Island and in Amundsen and Coronation gulfs (Figures 3c and 3d). Finally, Log(Al/Ca) is used as a sediment source and transport agent indicator. Indeed, higher Log(Al/Ca) values are found in the West Province for surface and basal sediments (Figures 3e and 3f), whereas lower Log(Al/Ca) values are mostly observed in the East Province in the surface and basal sediments.

##### 3.1.2. Grain Size Distribution

The mean surface and basal grain size in the study area do not depict great variability and are mainly composed of silts. Indeed, the mean surface sediment grain size expressed on the phi scale ranges from 9.0 (clay) to 7.0 (fine silt) whereas the minimum phi values are found in the Coronation Gulf. The surface sample grain size distribution shows a general West-East trend with finer grains (8–9  $\Phi$ ) in the western part and coarser grains (<8  $\Phi$ ) in the eastern part (Figure 4a). The basal sample grain size depicts a coarser grain size near to the Mackenzie mouth (~8.5  $\Phi$ ), whereas the grain size in the rest of the western and eastern parts generally become finer (7.5  $\Phi$ ) (Figure 4b).

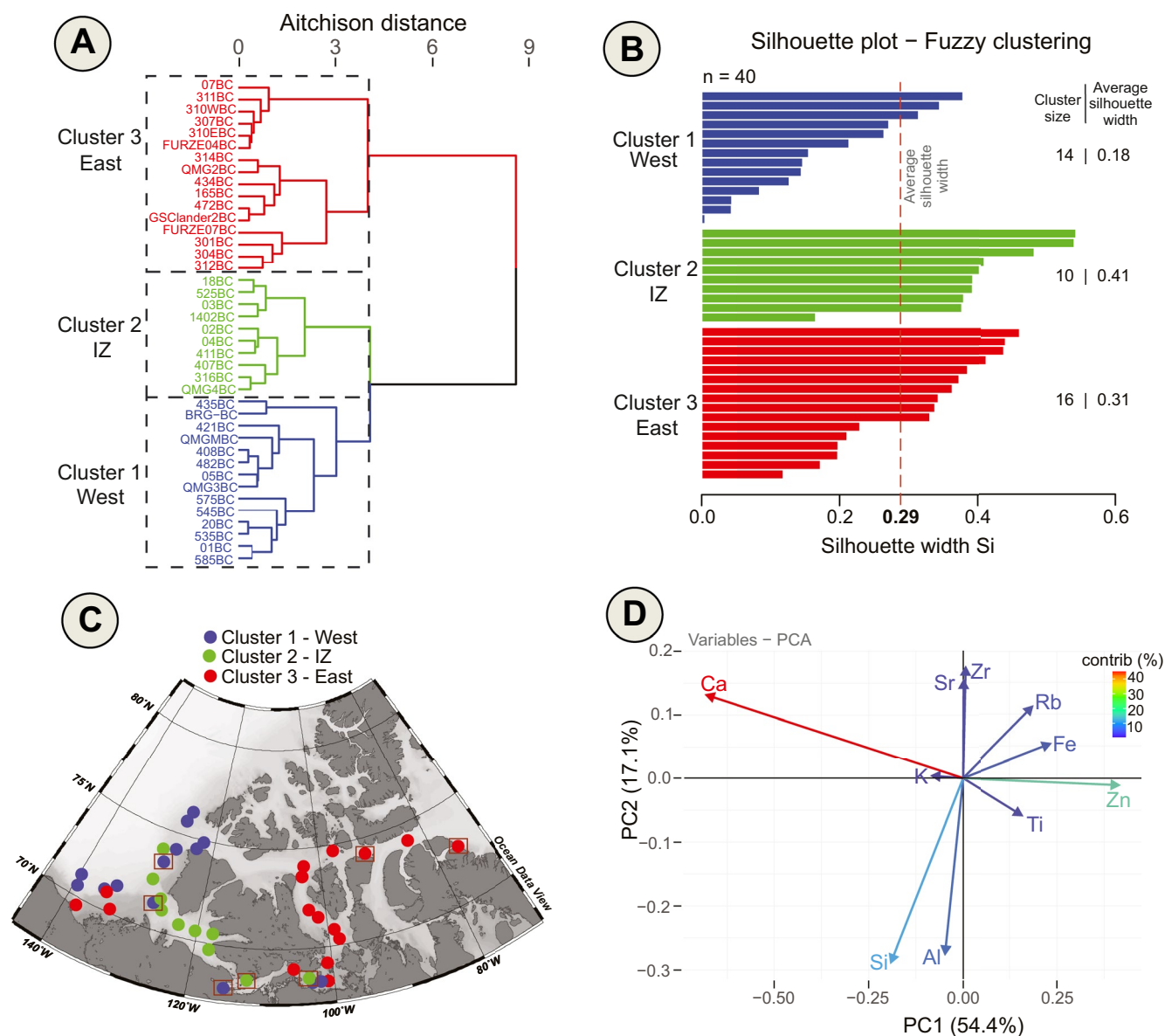


**Figure 2.** (a) Clustering dendrogram obtained by applying Ward clustering algorithm on the Professional X-ray fluorescence (pXRF) major element data (Ti-Mn-Fe-Al-Si-K-Ca). (b) Silhouette plot resulting from the fuzzy clustering analysis of the surface samples based on the pXRF major element data. 100% of the sediment samples are correctly classified. However, cluster 1 (West province) is mostly represented by samples with below-average silhouette width values ( $<0.29$ ) likely suggesting mixing of sediment provenance. (c) Map of the three clusters, which point out the three geochemical provinces. The red rectangle on stations correspond to  $^{210}\text{Pb}$  dated cores. (d) Biplot of the first principal component versus Second principal component obtained on the pXRF data. Note that Mn is removed from the principal component analysis because of its strong influence on geochemical variability.

Generally, sorting is better as the mean grain size decreases, especially in the West province surface sediments (Figure 4c). The most poorly sorted sediments are found in the East province and near the M'Clure Strait (545-BC and 20-BC).

### 3.1.3. Sediment Color

The presence of detrital carbonates in the eastern part of the CAA, more precisely in the Victoria Strait and M'Clintock Channel can be determined by a whiter sediment color expressed by higher  $L^*$  values (Figures 5a and 5b).  $L^*$  values are higher at the base than at the surface for these regions except for M'Clure Strait. In fact, higher  $L^*$  values for basal sediment, especially those found in the East province, appear to coincide with increases in the inorganic carbonate contents (Figures 5g and 5h), as well as decreases in the

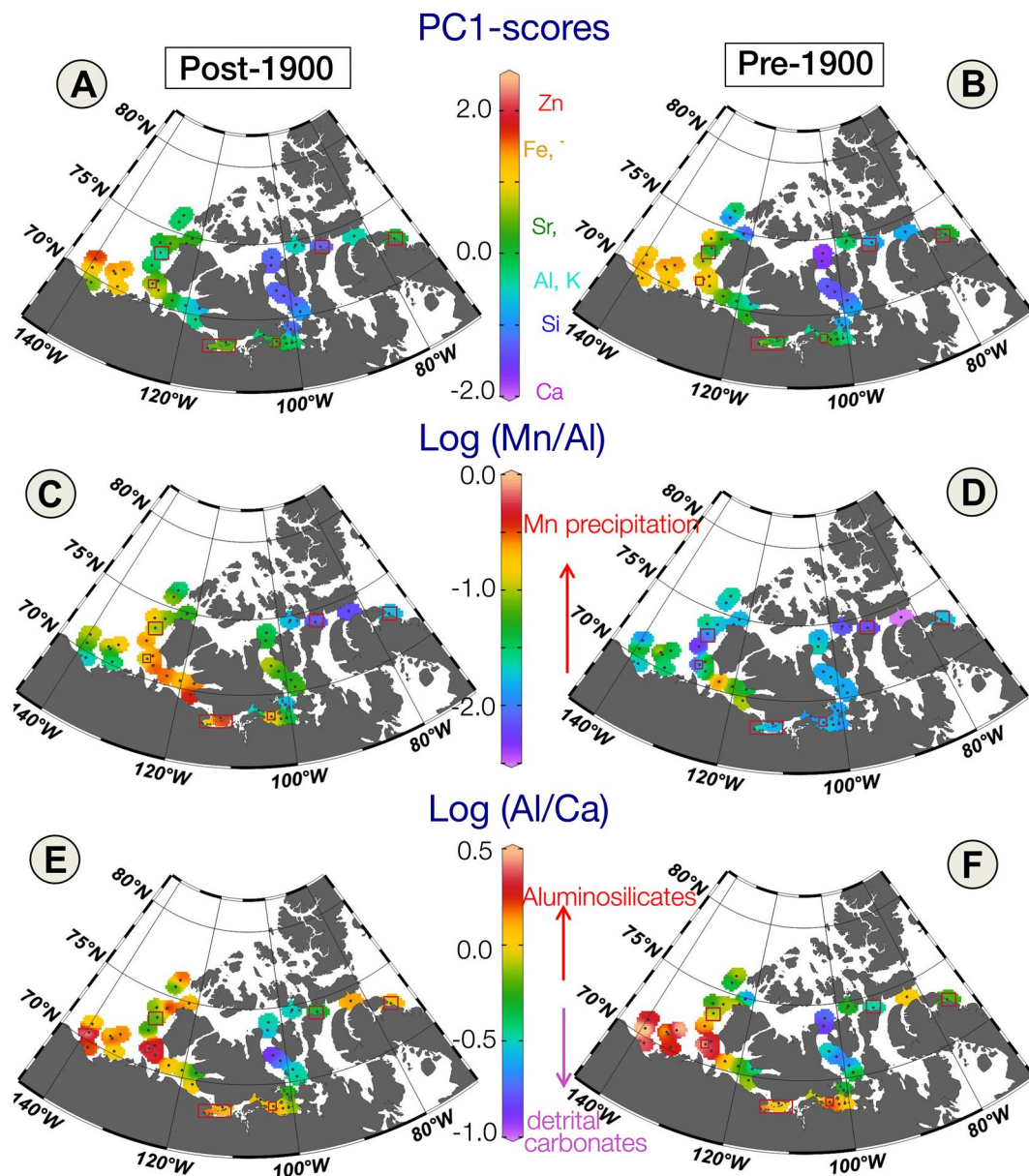


**Figure 3.** (a), (b) Map of first principal component scores derived from pXRF major elements data of surface (post-1900) and basal (pre-1900) sediment samples. Spatial distribution of  $\text{Log}(\text{Mn}/\text{Al})$  (c), (d) and  $\text{Log}(\text{Al}/\text{Ca})$  (e), (f) for surface (post-1900) and base (pre-1900) samples. High Mn concentrations are observed in surface samples located in the south of Banks Island, the entrance of Amundsen Gulf and part of Coronation Gulf. Al concentrations are higher in the Canadian Beaufort Shelf and Queen Maud Gulf, while Ca show higher concentrations in the M'Clintock Channel. The red rectangle on stations correspond to  $^{210}\text{Pb}$  dated cores.

$\text{Log}(\text{Al}/\text{Ca})$  ratios (Figures 4e and 4f) corresponding to the presence of detrital carbonates. Furthermore,  $a^*$  values tend to be higher in the Amundsen (southern area), Coronation and Queen Maud gulfs as well in M'Clintock Channel, both at the surface and at the base, representing a predominance of reddish sediments (Figures 5c and 5d). These higher values seem to correspond to high K contents instead of Fe or Mn (linked to Fe-Mn oxyhydroxide phases; Gamboa et al., 2017; Figure S6), most likely suggesting the presence of high potassium feldspars contents in these areas (e.g., Belt et al., 2010).

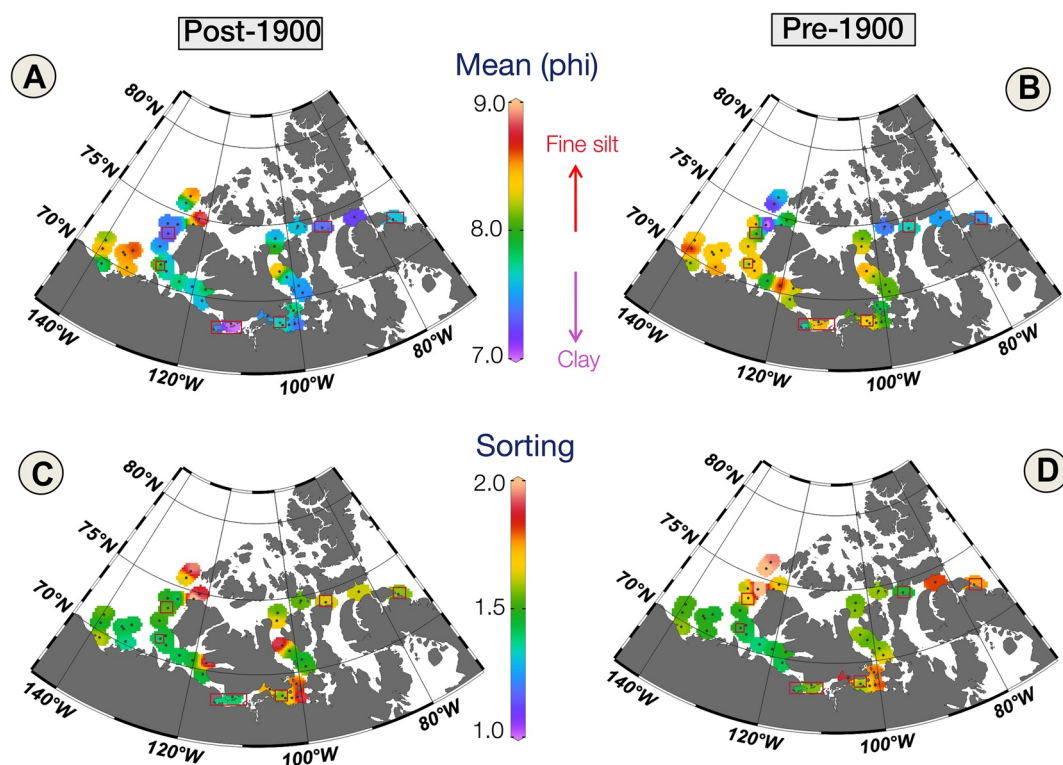


**Figure 4.** Spatial distribution of mean grain size (a), (b) and sorting (c), (d) for surface (post-1900) and basal (pre-1900) sediment samples from the Canadian Arctic Archipelago.

### 3.1.4. Carbonate and Inorganic Carbon Contents

Figures 5e–5h illustrates the organic and inorganic carbon concentrations in the study area. In the surface samples, the organic carbon content distribution shows higher concentrations in the West and along the Lancaster Sound (Figure 5e), whereas the organic carbon of basal samples decreases in the Mackenzie Shelf/Slope area (Figure 5f). On the other hand, the eastern area is characterized by higher contents of inorganic carbon for surface and basal sediments (Figures 5g and 5h). Inorganic carbon shows high positive correlation with Ca concentrations in all provinces (Figure S6), supporting the use of Ca as a proxy for detrital carbonate.

### 3.1.5. Organic Carbon Sources

The East province is first characterized by  $\delta^{13}\text{C}$  values ranging from  $-22\text{‰}$  to  $-23\text{‰}$  in surface sediments and from  $-24\text{‰}$  to  $-26\text{‰}$  at the base and second by C/N ratios between 5 and 10 in surface sediments and between 5 and 20 in basal sediments (Figure 6). The West province is characterized by more strongly negative  $\delta^{13}\text{C}$  values (from  $-24\text{‰}$  to  $-26.5\text{‰}$  at the surface and from  $-26\text{‰}$  to  $-30\text{‰}$  at the base) and higher C/N values (from  $\sim 7$  to 14 in surface sediments and from 5 to 25 at the base). Figure 6 reveals a west-east trend with more terrigenous OM in the West, more marine OM in the East and a mixing between marine and terrigenous OM in the intermediate zone. These results agree with  $\delta^{13}\text{C}$  and C/N data reported for surface sediments from the CAA (CASCADE; Goñi et al., 2013; Martens et al., 2020) and southern Beaufort Sea—Amundsen Gulf region (Couture et al., 2018; Goñi et al., 2005; Guo et al., 2007; Magen et al., 2010). Finally, the data also reveal that  $\delta^{13}\text{C}$  values become highly depleted (from  $-25\text{‰}$  to  $-29\text{‰}$ ) whereas C/N ratio values are higher (7–25) between the surface and the base of the sediment cores (Figure 6), suggesting an enhanced terrigenous organic matter inputs, and thus, a period of increasing freshwater discharge.

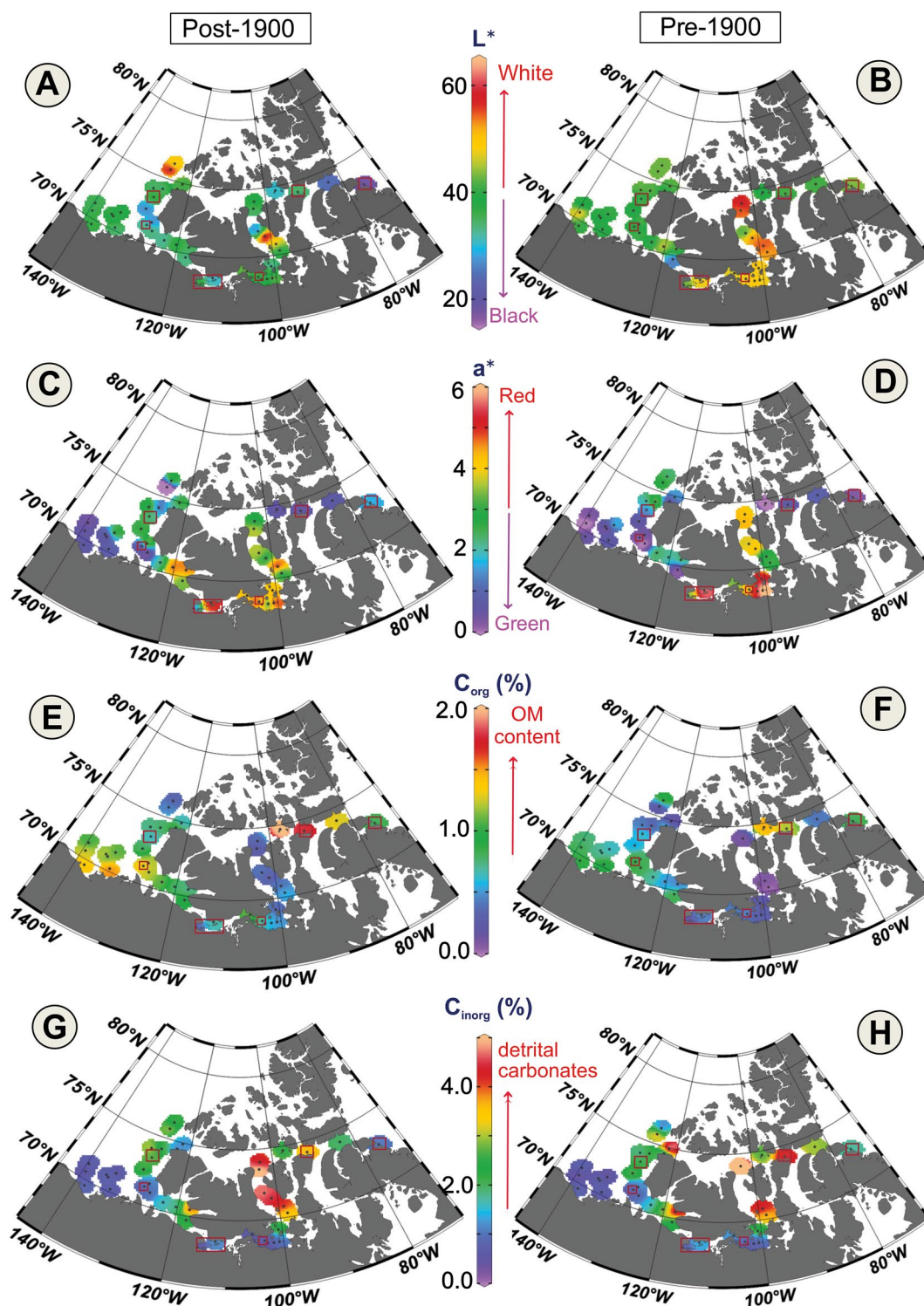


**Figure 5.** Spatial distributions of color indices  $L^*$  (a), (b) and  $a^*$ (c), (d) as well as of organic carbon (e), (f) and inorganic carbon (c), (d) contents for the surface (post-1900) and basal (pre-1900) sediment samples from the Canadian Arctic Archipelago. The red rectangle on stations correspond to  $^{210}\text{Pb}$  dated cores.

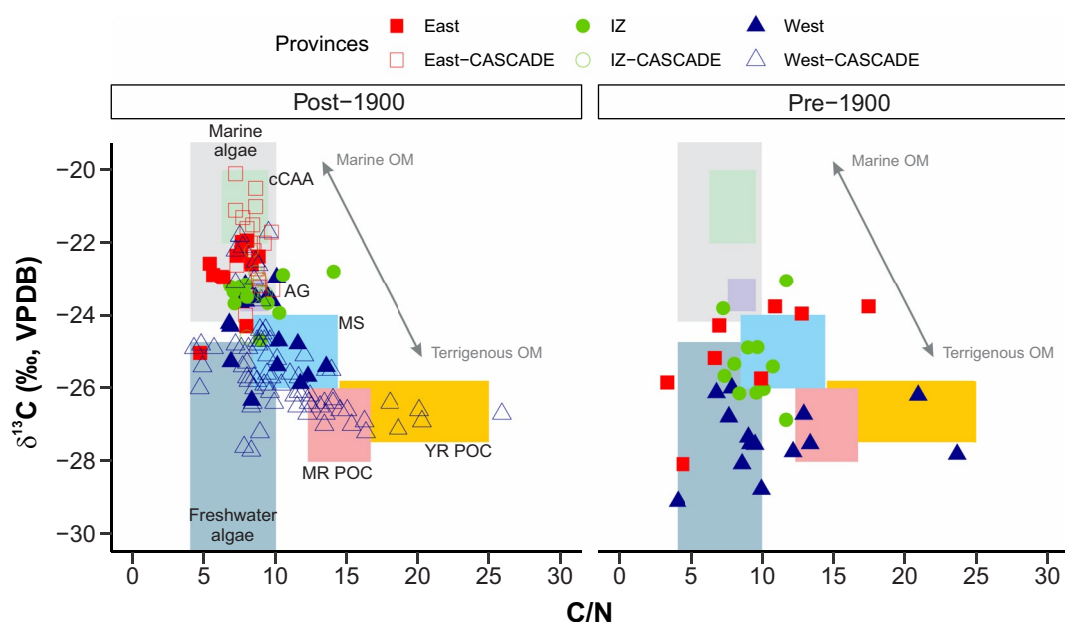


**Figure 6.** Relationship between C/N and  $\delta^{13}\text{C}$  values for the surface (post-1900) and basal (pre-1900) sediment samples from the Canadian Arctic Archipelago. Three distinctive clusters of C/N and  $\delta^{13}\text{C}$  values are highlighted and correspond to the three geochemical provinces defined by clustering analysis: West, Intermediate Zone (IZ) and East. The compositional ranges of potential marine and freshwater organic carbon sources (Lamb et al., 2006), surface sediments from the Circum-Arctic Sediment CARbon DatabasE (Martens et al., 2020), suspended particulate organic matter from the Mackenzie River (Goñi et al., 2005) and Yukon River (Couture et al., 2018; Guo et al., 2007), surface sediments from the Mackenzie Shelf and Amundsen Gulf (MS and AG, respectively; Magen et al., 2010) and central Canadian Arctic Archipelago (Goñi et al., 2013) are plotted also for comparison.

## 3.2. Magnetic Properties

### 3.2.1. Magnetic Concentration

To more closely examine the magnetic grain concentration, a concentration-dependent parameter is used: magnetic susceptibility ( $k_{LF}$ ; Figures 7a and 7b). Generally, the intermediate zone surface samples show higher values in magnetic susceptibility ( $k_{LF} > 25 \times 10^{-5}$  SI) than samples from anywhere else ( $k_{LF} = 5\text{--}10 \times 10^{-5}$  SI). This feature suggests a higher concentration of ferrimagnetic material in the intermediate zone, whereas lower magnetic susceptibilities recorded in the Western and Eastern areas could be due to the higher organic matter contents in the West and the higher detrital carbonate concentration in the East. Finally, magnetic susceptibility is mainly lower in the base than in the surface sediment samples.

Difference in the magnetic susceptibility values between the low and high frequencies is negligible, suggesting the absence of superparamagnetic grains (Table S1). In addition, the magnetic mineralogy in the CAA is mainly dominated by minerals with low coercivity, such as magnetite. This observation is particularly supported by the pseudo S-ratios, which are generally  $>0.9$ . Indeed, more magnetite seems to be present in Barrow Strait and Lancaster Sound for the surface samples (Figure 7c), whereas in the base samples, pseudo S-ratio data increase and almost all samples values close to 1, except for those from the southern M'Clintock Channel, Coronation Gulf and M'Clure Strait (Figure 7d).

On the other hand, the median destructive field of isothermal remanent magnetization ( $\text{MDF}_{IRM}$ ) reveals higher values in M'Clintock Channel for surface and base samples (Figures 7e and 7f). Otherwise,  $\text{MDF}_{IRM}$  values tend to decrease from  $\sim 30$  to  $\sim 20$  mT between the surface and the base in samples from the M'Clure Strait, the Amundsen Gulf and the west of Banks Island areas.

### 3.2.2. Magnetic Grain Size

A coarsening magnetic grain size trend is mainly observed between the surface and basal sediments but also from West to East (Figure 7g). Most samples are included in the pseudo-single domain (PSD) range

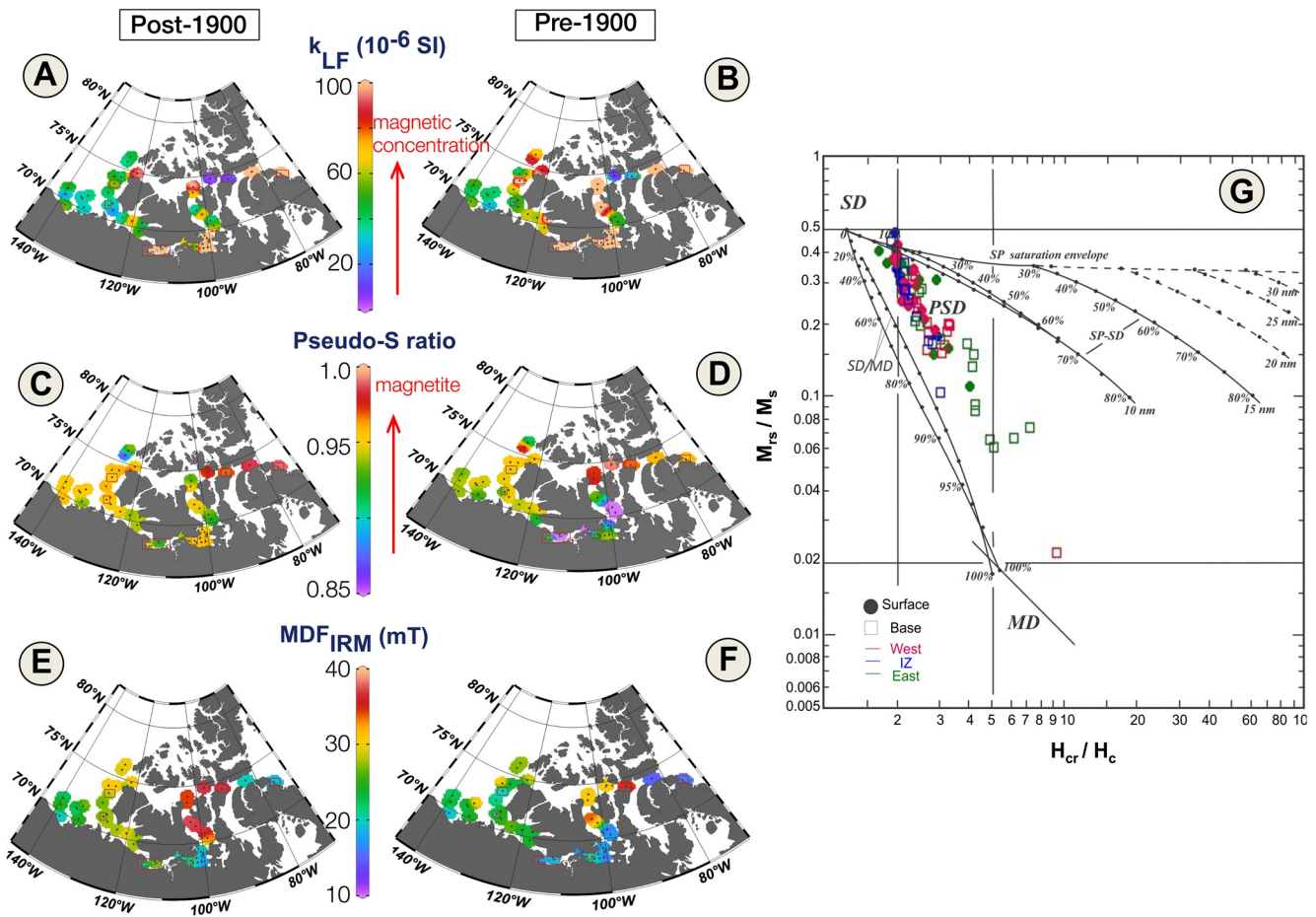


**Figure 7.** Spatial representations of magnetic properties from surface (post-1900) and basal (pre-1900) sediments from the Couture et al., 2018: (a) and (b) for magnetic susceptibilities ( $k_{LF}$ ). (c) and (d) illustrate the pseudo S-ratio (Stoner & St-Onge, 2007). The Median Destructive Field of the isothermal remanent magnetization ( $MDF_{IRM}$ ) is represented in panels (e) and (f). The red rectangle on stations correspond to  $^{210}\text{Pb}$  dated cores. Finally, Day plot (Day et al., 1977) for the surface and basal samples from the CAA is illustrated in panel (g). The mixing reference lines for single and multi-domain (SD and MD) are from Dunlop (2002). Frequency dependence and magnetic mineralogy.

and seem to be aligned to the theoretical single and multi-domain (SD + MD) mixing line. A larger contribution of coarser MD magnetite grains and other minerals is evident for the East basal sediments and one West basal sample (AMD 2016-805-20BC). Otherwise, the rest of the samples are dominated by finer PSD magnetite grains.

### 3.3. Relationships Between Magnetic Properties, Grain Size and Elemental Geochemistry

The relationships between the different properties are established by using bivariate graphs (Figure 8). First, relation between the mean phi grain size and skewness shows that surface sediments from the East and IZ Provinces are mostly characterized by coarse detrital grain sizes with asymmetric distributions (Figure 8a). In turn, surface sediments from the West Province and the majority of base sediment samples show the opposite trend. In addition, the relationship between the magnetic grain size ( $M_{rs}/M_s$ ) and the elemental geochemistry ratio (Figure 8b) reveals a west-east trend where surface samples from the East Province are mostly characterized by fine magnetic grains (high  $M_{rs}/M_s$  ratios) and high contents of detrital carbonates (low  $\text{Log}[\text{Al}/\text{Ca}]$  ratios), whereas the West and IZ Provinces are influenced by high aluminosilicate concentrations.



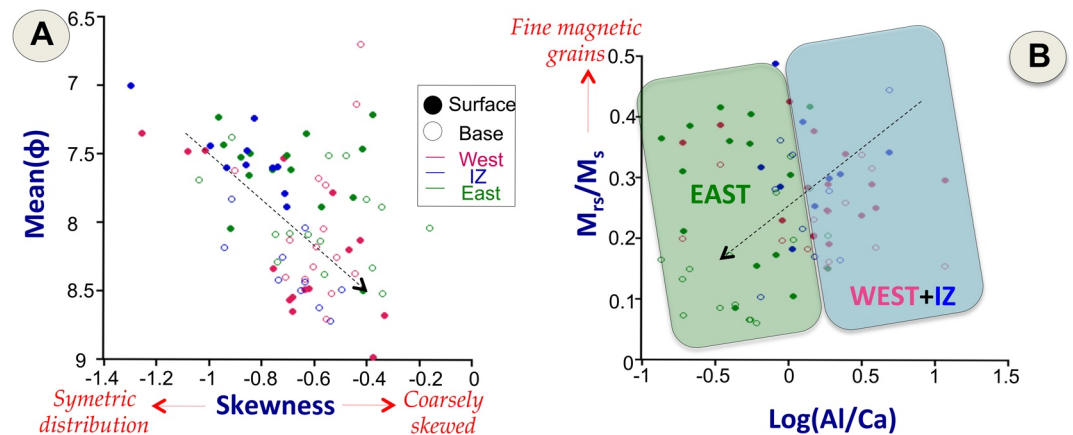


**Figure 8.** Relationship between: (a) sediment grain size characteristics such as mean grain size in phi-scale and skewness and (b) magnetic and geochemistry parameters as  $\log(Al/Ca)$  and magnetic grain size  $M_{rs}/M_s$ .

### 3.4. Lead-210 Dating

Clear radioactive decay is observed in  $^{210}Pb$  data of seven box cores and allows visual determination of the value of the supported  $^{210}Pb$  and excess  $^{210}Pb$  (Figure 9). No homogenized  $^{210}Pb_{ex}$  activities are observed at

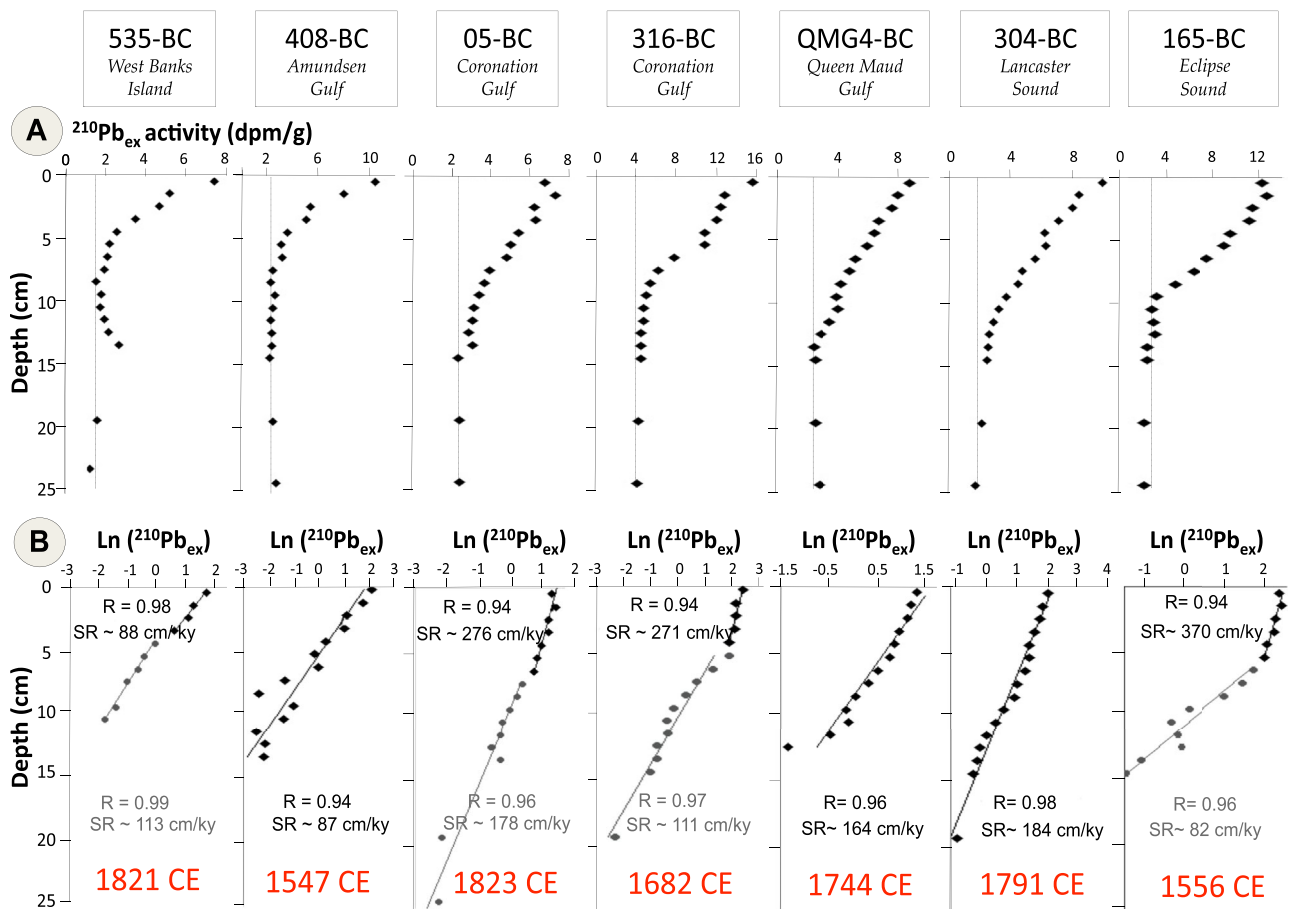


**Figure 9.** (a)  $^{210}Pb$  chronology of selected box cores from the Canadian Arctic Archipelago. Total activity of the  $^{210}Pb$  (dpm/g) and vertical dashed lines characterized supported  $^{210}Pb$  was represented in the first row. (b) Gray and black  $\ln$  (excess of  $^{210}Pb$  activity) plot symbols distinguish two slopes and thus different sedimentation rates which are both used to estimate the basal age (CE) of the cores (red text).

the top of these cores (Figure 9b), suggesting minimal bioturbation and sediment deposition in non-reworked environments (e.g., Kuzyk et al., 2013; Xu et al., 2015). The downcore excess  $^{210}\text{Pb}$  linear regressions indicate that the highest average SR are recorded near the mouths of Coppermine and Ellice rivers (Coronation and Queen Maud gulfs; 271–276 cm/ka), in zones with enhanced sea-ice rafting (Barrow Strait-Lancaster Sound; 184 cm/ka), and in an area influenced by glacial discharges (Eclipse Sound; 370 cm/ka). While the lowest average SR are recorded in Amundsen Gulf (87 cm/ka) and west Banks Island (88 cm/ka), where sediments are mainly supplied from coastal cliff erosion (e.g., Gamboa et al., 2017). Basal sediments of the seven box cores have ages ranging from ~1550 to 1820 CE, providing an opportunity to compare post-1900 conditions with those of the LIA (~1500–1900 CE; Jones & Mann, 2004). Overall, these new SR estimates are similar to and complement the different data already obtained (summarized in Figure S5) in the Mackenzie Shelf/Slope (Bringué & Rochon, 2012; Durantou et al., 2012; Kutos et al., 2021; Richerol et al., 2008), Coronation Gulf (Pieńkowski et al., 2011, 2017), Queen Maud Gulf (Kuzyk et al., 2013), Victoria and Barrow straits (Belt et al., 2010; Ledu, Rochan, de Vernal, Barletta, & St-Onge, 2010; Ledu, Rochan, de Vernal, & St-Onge, 2010; Pieńkowski et al., 2013; Vare et al., 2009), and Peel Sound (Kuzyk et al., 2013).

## 4. Discussion

### 4.1. Sedimentary Provinces and Processes

As a result of the statistical analysis, together with sedimentological, magnetic properties and the color of the surface and basal sediments, three main provinces and their distinct sedimentary compositions and dynamics are described below and summarized in Figure 10.

#### 4.1.1. The West Province

The surface sediments (post-1900) of the West Province (Mackenzie Shelf/Slope, west Banks Island and the M'Clure Strait; cluster 1) are mainly characterized by: fine detrital grains, detrital element (Fe-Rb-Ti-Zn) associations, a dominance of aluminosilicates (high  $\text{Log}[\text{Al}/\text{Ca}]$  ratios), and a moderate positive correlation between Mn, Fe, and K (Figure S6a), implying high detrital inputs delivered particularly by rivers. In this province, PSD magnetite and magnetically soft minerals suggesting the presence of low-coercivity minerals (Figures 7c and 7g) with a  $\text{MDF}_{\text{IRM}}$  of ~25 mT are noted, but even if magnetite is present, the magnetic susceptibility ( $k_{\text{LF}}$ ; Figure 7a) remains relatively weak. This feature may be explained by the dilution of magnetic minerals by the large terrestrial OM supply (Figures 5e, 5f and 6) coming from the Mackenzie River discharge (Gamboa et al., 2017; Macdonald et al., 1998; Magen et al., 2010). The heterogeneous sedimentary composition (i.e. mixture of sediments rich in aluminosilicates and detrital carbonates; Figures 2b and 2c) within the Mackenzie Shelf/Slope, the relatively symmetric and skewed grains and the constant mean grain size (Figure 4a) support the idea that the post-1900 sedimentation in this area is thus mainly dominated by the Mackenzie River discharge (Deschamps, Montero-serrano, et al., 2018; Deschamps, St-Onge, et al., 2018; Gamboa et al., 2017; Hill et al., 1991). Detrital inputs from the Mackenzie River derive mainly from the Interior Platform, where Cambrian to Cretaceous shales, sandstones, and limestone are cropping out (Deschamps, Montero-serrano, et al., 2018; Gamboa et al., 2017; Millot et al., 2003). Moreover, differences in the sedimentary records observed within this province suggest that the Mackenzie plume influence is not strong enough to be the only common factor controlling the recent sedimentary processes in west Banks Island and M'Clure Strait areas. Indeed, in addition to the high contents of organic carbon found in west Banks Island, confirming the influence of Mackenzie River discharge, poorly sorted fine silts and detrital carbonate contents are higher than those on the Mackenzie Shelf/Slope. This difference likely suggests a modern supply by coastal cliff erosion of Quaternary dolomite-rich tills, in agreement with other studies in this area (Belliveau, 2007; Gamboa et al., 2017; Lewkowicz & Way, 2019; O'Brien et al., 2006). Finally, in the M'Clure Strait region, the high contents of carbonate and aluminosilicate minerals and the mixture of terrestrial and marine OM observed in surface sediments suggest sedimentation influenced by the mixing of sedimentary material produced locally (autochthonous) and that transported from outside the region (allochthonous) (Howell & Brady, 2019). Indeed, we assume that coastal erosion of Banks and Prince Patrick islands added to the presence of several small Banks Island rivers (such as the Bernard, Big and Thomsen Rivers; Figure 1a) promote inputs of such carbonate- and aluminosilicate-rich sediments, which are subsequently brought into the M'Clure Strait by sea-ice transport and coastal currents (e.g., Darby, 2003).

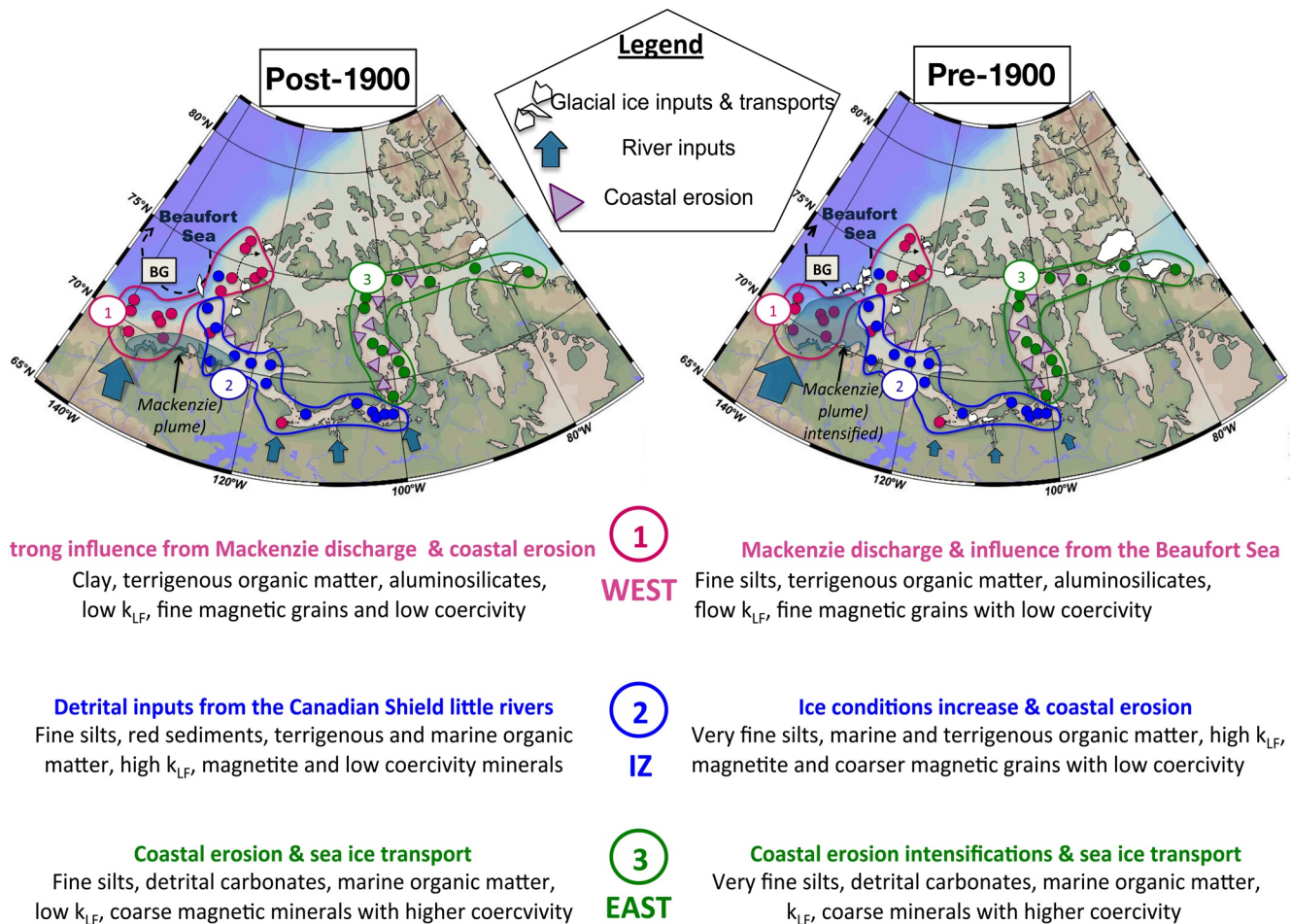


**Figure 10.** Summary of the sedimentary processes involved from each province during the pre- and post-industrial periods. Note that the Pre and Post-1900 ice extents are only conceptual.

The main sedimentary properties within the West Province remain substantially similar for the basal samples, which describe pre-1900 conditions. Indeed, this province remains characterized by a high  $\text{Log}(\text{Al}/\text{Ca})$  ratio associated with a terrigenous OM inputs, the presence of SD/PSD magnetite and low-coercivity minerals, along with a constant weak magnetic susceptibility. The stable  $\text{MDF}_{\text{IRM}}$  reflects a similar magnetic mineralogy (Figure 7f), but the coarser magnetic grain sizes illustrated by the Day plot (Figure 7g) reveal a possible change in the magnetic grain size (Özdemir & Dunlop, 1997; Stoner & St-Onge, 2007). Nevertheless, some differences can also be observed involving changes in the sedimentary processes. The detrital grain size is coarser near the Mackenzie River mouth and becomes finer in surrounding areas and to the north of Banks Island in basal sediment samples (Figure 4b), together with coarsely skewed grains. These changes in pre-1900 sediments are also accompanied by an increase in aluminosilicate contents (higher  $\text{Log}[\text{Al}/\text{Ca}]$  ratios; Figure 3f) to the north of Banks Island as well as the slight  $\% C_{\text{inorg}}$  decrease (Figure 5h) to the west of Banks Island. Based on previously published mineralogical, geochemical and palynological studies performed on the Mackenzie Shelf and Slope during the Late Holocene (e.g., Deschamps, Montero-serrano, et al., 2018; Durantou et al., 2012; Hanna et al., 2018; Richerol et al., 2008), we hypothesize that the sedimentological changes recorded in pre-1900 sediments in this province were likely driven by an increase and a wider influence of the Mackenzie River discharge along the Canadian Beaufort margin.

On one hand, the results of the dated cores 408-BC and 535-BC show a magnetic concentration increase from post-1900 to pre-1900 periods (from 20 to  $50 \cdot 10^{-6}$  SI for 408-BC and from 50 to  $70\text{--}80 \cdot 10^{-6}$  SI for 535-BC; Figure 7) as well as detrital grain size (Figure 4),  $\text{Log}(\text{Al}/\text{Ca})$  values, a constant pseudo S-ratio (close to 1; Figure 7) and inorganic carbon content and finally, a decrease of OM content (Figure 5). These observations

may indicate a dilution by organic matter which is more important in the West Province during the pre-1900 period. On the other hand, palynological studies all around the area suggest that colder sea surface conditions, higher-than-average sea-ice cover, and enhanced Alaskan Coastal Current (ACC) flow prevailed during the LIA period (e.g., Bringué & Rochon, 2012; Durantou et al., 2012; Richerol et al., 2008). These features lead us to speculate that the climate and marine conditions during the LIA likely fostered the recurrent incorporation of Mackenzie Shelf sediments rich in coarse-grained magnetite into the sea ice (a process known as suspension freezing; Darby, 2003; Reimnitz et al., 1990, 1993) and their subsequent entrainment towards the Amundsen Gulf entrance and northern Banks Island via the ACC (e.g., Lin et al., 2020). This hypothesis is also supported by the increase in asymmetric grain distribution and magnetic grain contents in basal samples from core 535-BC, implying different depositional processes such as sea-ice transport and river discharges and the work of oceanic currents.

#### 4.1.2. The Intermediate Province

The IZ (Amundsen, Coronation and Queen Maud gulfs; cluster 2) acts as a transitional zone between the West and East Provinces (Figures 2a–2c and 10). The surface sediments are defined by common characteristics: Si-Al-Zr-Sr-K contents, high concentrations of Mn and Al (associated with aluminosilicates) and a mixture of terrigenous and marine OM. Magnetically, the pseudo S-ratio values indicate the presence of low coercivity minerals in the Coronation and Queen Maud gulfs (Figure 7c). In addition, the high magnetic susceptibilities, as well as the low  $\text{MDF}_{\text{IRM}} \sim 15$  mT suggest the presence coarser of magnetic grains. The high concentrations of Mn are mainly observed in Amundsen and Coronation gulfs (Figure 3c). In these regions, Mn shows a moderate positive correlation with Al, K, and  $C_{\text{org}}$  and a low correlation with Fe and  $a^*$  (Figure S6a), indicating an association with continental particulate matter derived from riverine input and/or coastal erosion (Macdonald & Gobeil, 2012). In fact, a well-oxygenated water column sustained by vertical turbulent mixing (strong winds and recurrent ice-free conditions) and high OM input foster ideal conditions for both the settling of Mn oxyhydroxides onto the seafloor via vertical particle flux and its subsequent reductive remobilization (Gamboa et al., 2017; Macdonald & Gobeil, 2012). Furthermore, some differences between Amundsen and Coronation gulfs are also noteworthy. The high contents of poorly sorted clay-size sediments ( $\sim 8 \Phi$ ), relatively high concentrations in terrestrial OM contents and low magnetic susceptibility found in the Amundsen Gulf reflect a modern sedimentation dominated by the strong influence of the far-reaching Mackenzie plume (Hill et al., 1991; Macdonald et al., 1998; Schell et al., 2008). In addition, the relatively high content of detrital carbonates observed in the Amundsen Gulf demonstrates a further contribution from the coastal cliff erosion process (Belliveau, 2007; Lewkowicz & Way, 2019) occurring to the south and west of Banks Island. Coronation and Queen Maud gulfs are in turn characterized by the predominance of detrital fine silts, asymmetric grain distributions, low concentrations of organic and inorganic carbon, high  $a^*$  values and high magnetic susceptibilities. On the other hand, the high  $\text{Log}(\text{Al}/\text{Ca})$  values and high positive correlation between  $a^*$  and K (Figure S6) in Coronation and Queen Maud gulfs indicate the presence of aluminosilicate-enriched sediments (particularly potassium feldspars and illite; Belt et al., 2010; Deschamps, Montero-serrano, et al., 2018). These observations suggest that local sedimentation is mainly influenced by surrounding rivers (such as Coppermine in the Coronation Gulf and Back, Hayes, Perry, Armark, Simpson, Hayes and Ellice rivers in the Queen Maud Gulf; Alkire et al., 2017), draining the Canadian Shield. All these observations explain the presence of the sediment samples from the mouth of Coppermine and Ellice rivers in the cluster 1 (West Province) instead in the IZ.

The basal sediments (pre-1900) display some similarities with those from the surface (post-1900): the elemental geochemistry is still dominated by the Si-Al-Sr-Zr-K association, the detrital grain size is generally finer,  $a^*$  remains governed by potassium feldspars, whereas the magnetic mineralogy shows decreases in magnetite contents based on the lower pseudo S-ratios (Figure 7d) as well as the slight decreases in the  $\text{MD-F}_{\text{IRM}}$ , which reveal coarser magnetic grain sizes. These similarities may suggest that the sediment sources remained the same and that some changes could be due to the contribution of different transport agents (such as sea-ice transport; Darby, 2003). Additionally, the lower  $\text{Log}(\text{Mn}/\text{Al})$  ratios, especially in Coronation and Queen Maud gulfs, and the high positive correlation between Mn and Fe (Figure S6b) suggest that Mn is likely reduced and remobilized at depth in sediments by diagenetic processes (e.g., Kobayashi et al., 2016). In these latter areas, the higher  $\text{Log}(\text{Al}/\text{Ca})$ , magnetic susceptibilities, higher pseudo S-ratios and concentrations of reddish sediments in the LIA interval of the dated cores 05-BC, 316-BC, and QMG4-BC may indicate more continental inputs from the Canadian Shield during the LIA, supplied by an enhanced river

discharges, coastal erosion and sea-ice transport. This hypothesis agrees with the studies of Pieńkowski et al. (2011, 2017) and Belt et al. (2010), which reconstructed colder conditions during the LIA with higher sea-ice extent and a shorter open-water season in these areas.

#### 4.1.3. The Eastern Province

Surface sediments (post-1900) of the Eastern Province mainly indicate the presence of fine silts ( $\sim 7.5 \Phi$ ) and a chemical composition generally dominated by calcium and marine OM. In addition, the magnetic properties reveal weak magnetic susceptibilities that intensify slightly and gradually eastward. The presence of low coercivity minerals (Figure 7c) such as SD magnetite (Figure 7c) is illustrated by  $MDF_{IRM} \sim 40$  mT that increases gradually eastward (Figure 7e). On the other hand, specific differences within this province can be observed. Victoria and Barrow straits dominantly show detrital carbonates supported by low  $\text{Log}(\text{Al}/\text{Ca})$  values and  $C_{\text{inorg}} > 5\%$ , suggesting that modern sedimentary processes are dominated by coastal erosion of Ordovician-Silurian carbonate-bearing rocks cropping out in Victoria, Prince of Wales and Somerset Islands as well as on the Brodeur Peninsula before they are ultimately transported by sediment-laden sea ice (Reimnitz et al., 1993). Moreover, the high contents of aluminosilicates and terrigenous OM inputs and the lower contents of detrital carbonate inputs in eastern Lancaster Sound can indicate that sediments are mainly transported by sea ice. The presence of glaciers on Devon Island and in Sirmilik National Park could have a local impact on settling by generating iceberg rafting and sediment-laden meltwater plume sediment supply.

The basal (pre-1900) sediment samples in this province are mainly characterized by a finer detrital grain size ( $\sim 8.5 \Phi$ ), poorer sorting, a high positive correlation between  $L^*$ ,  $a^*$ , and Ca (Figure S6b), a dominant association of Ca-Si with relatively weak magnetic susceptibilities that increase in the M'Clintock Channel and more terrigenous sediment inputs than the surface sediments. Based on these results, we hypothesize that the sediment color ( $L^*$  and  $a^*$ ) in this province is mainly driven by mineral composition (mainly detrital carbonate, quartz and potassium feldspars; Belt et al., 2010). Compared to the surface sediments (post-1900), the basal sediments have the magnetic mineralogy that is dominated by higher-coercivity minerals and a mixture of PSD/MD magnetite. On the other hand, the increase in magnetic susceptibilities in the M'Clintock Channel, the pseudo S-ratios close to one and the increase in magnetic grain sizes, suggest the presence of a higher concentration of coarser magnetite during the pre-1900 period. Bischof and Darby (2000) observed higher magnetite concentrations (up to 36%) in the Fe oxide fraction of tills samples from the northern Viscount Melville Sound (Figure 1a). Thus, we suggest that magnetite-rich sediments from the Viscount Melville Sound area are probably incorporated into the sea ice during its formation and subsequently transported by drifting ice to the entrance of the M'Clintock Channel. Furthermore, the relatively lower OM and higher detrital carbonate contents correlated with whiter sediments in M'Clintock Channel suggest more pronounced contributions of coastal erosion and sea-ice sediment transport during pre-1900 conditions than under the post-1900 ones. In addition, the high  $C_{\text{org}}$  values (1.5%–2%) recorded in the Barrow Strait relative to the rest of the province in both surface and basal sediment samples suggest enhanced primary productivity probably related to the recurrent polynya formation in this area (e.g., Hannah et al., 2009; Steffen, 1986). The occurrence of polynyas in Barrow Strait area seems to be connected with the location of a wintertime ice plug (fast-ice arch) in the south of Cornwallis Island (Steffen, 1986). In this latter area, fine-grained and poorly sorted sediment samples from the LIA interval in the dated core 304-BC show low  $\text{Log}(\text{Al}/\text{Ca})$  and high  $C_{\text{inorg}}$  (up to 4%) values, similar to the post-1900 sediment samples, suggesting similar-to-modern sedimentary conditions during LIA in Barrow Strait area. Few variations in sedimentological and geochemical proxies since 1550 CE have also been reported in a nearby core from Barrow Strait (core 2005-804-004BC; Ledu, Rochon, de Vernl, & St-Onge, 2010), consistent with our interpretations. Note that since no  $^{210}\text{Pb}$ -dated cores are available in M'Clintock Channel area (Figure S5), we are not able to conclude about the impact of the cooler LIA conditions on the sedimentary dynamics in this region.

In Eclipse Sound (southern Bylot Island), LIA samples from the dated core 165-BC are characterized mainly by the association of Si-Al-Zr-Rb-Ti, high magnetic susceptibilities, and fine-grained and poorly sorted sediments. Previously palynological lake studies around Bylot Island (e.g., Gajewski & Frappier, 2001; Gajewski et al., 1995; Peros & Gajewski, 2008; Zabenskie & Gajewski, 2007) suggest that cold climate conditions prevailed during the LIA in this area. In this context and because Bylot Island glacier drains Archean gneiss from the Canadian Shield in the east part as well as Mesozoic-Cenozoic siliciclastic rocks in west part, we

hypothesize that an enhanced glacier activity during the LIA period likely promoted an enhanced input of poorly sorted detrital sediments of mixed origin (i.e., from Archean gneiss and siliciclastic rocks).

#### 4.2. Methodological and Sediment Dynamic Implications

Methodologically, our study illustrates that by combining the magnetic, geochemical and sedimentological properties, together with cluster and spatial analyses, we can determine provenance and sedimentary processes that operate within the CAA. Given the challenges of dating marine sedimentary sequences in the Arctic Ocean, this study also allows the dating of seven new box cores from west Banks Island, Lancaster and Eclipse sounds, and Amundsen, Coronation and Queen Maud gulfs to improve the Arctic chronology mosaic. In addition, the high number of box cores used in this study considerably extends the spatial coverage of sedimentary records available across the marine CAA, allowing us to compare pre- and post-1900 sedimentary conditions and provide clues with those of the LIA period. In terms of sedimentary dynamics, this study points out the variability of sedimentary processes in each part of the CAA taking place during the pre- and post-industrial periods. Post-1900 sedimentary processes are mainly influenced by the Mackenzie River discharge and its far-reaching plume in the Mackenzie Shelf/Slope and the Amundsen Gulf, small CAA rivers draining the Canadian Shield, coastal erosion and sediment-laden sea-ice in the Banks Island area, the M'Clure Strait and the East Province, whereas pre-1900 sedimentary processes suggest an intensification of the continental runoff in the West (Mackenzie River) and IZ (e.g., Coppermine and Ellice rivers) and more intense sea-ice conditions along with sediment-laden sea ice and coastal erosion in the IZ and eastern CAA.

### 5. Conclusions

The regional heterogeneity in sedimentary processes that operate within CAA during the pre- and post-industrial periods was investigated through magnetic, geochemical and sedimentological analyses of 40 surface and 40 basal sediments throughout the CAA. The following conclusions are detailed below:

1. The multiproxy analysis allows the identification of three sedimentary provinces: (a) the West Province (the Mackenzie Shelf/Slope, western Banks Island and M'Clure Strait) is typified by detrital associations (Fe-Rb-Ti-Zn), important terrestrial OM inputs and high aluminosilicate inputs; (b) the Intermediate Zone (Amundsen, Coronation and Queen Maud gulfs) is distinguished by Si-Al-Zr-Sr-K associations, Mn oxyhydroxide precipitation (particularly in the recent period), high magnetic susceptibilities and a mixture between marine and terrestrial OM contents; and (c) the Eastern Province (the Queen Maud Gulf, Victoria and Barrow straits and Lancaster/Eclipse sounds) is characterized by high detrital carbonate inputs, marine OM contents, and low magnetic grain concentrations.
2. Pre- and post-industrial sedimentary processes are mainly influenced by the Mackenzie River discharge and its far-reaching plume in the Mackenzie Shelf/Slope and the Amundsen Gulf areas and by small CAA rivers draining the Canadian Shield in Coronation and Queen Maud gulfs, whereas the Banks Island area, the M'Clure Strait and the Barrow Strait/Lancaster Sound are mostly characterized by coastal erosion and sediment-laden sea ice. In Eclipse Sound, sedimentation is mainly driven by Bylot Island glacier dynamics.
3. Seven  $^{210}\text{Pb}$ -dated box cores from of three determined provinces suggest an intensification of the continental runoff in the West (Mackenzie River) and IZ (Coppermine and Ellice rivers) and more intense sea-ice conditions along with sediment-laden sea ice and coastal erosion in the IZ and the eastern CAA during the LIA period.
4. Our geochemical proxy  $\text{Log}(\text{Al}/\text{Ca})$  ratio derive from pXRF can be successfully used to track changes in the sedimentary sources within the CAA, where Al is associated with aluminosilicate minerals discharged by rivers and Ca is linked to detrital carbonates, coastal erosion and sediment-laden sea ice.

Finally, this study provides a basis for using the sedimentological, geochemical and magnetic signatures of longer sediment records from the CAA to reconstruct variations in sediment dynamics related to late Quaternary climatic and oceanographic changes.

## Data Availability Statement

All analytical data presented are available in the PANGAEA data repository: <https://doi.pangaea.de/10.1594/PANGAEA.910671>.

## Acknowledgments

The authors sincerely thank the captain, crew and scientific participants of the 2016 ArcticNet expedition onboard the CCGS Amundsen for the recovery of the cores used in this study. The authors also thank Marie-Pier St-Onge (RQM), Quentin Beauvais (ISMER-UQAR), Mathieu Babin (ISMER-UQAR) and Bassam Ghaleb (GEOTOP) for all their technical support and advice in the laboratory. Financial support for this research project was provided by ArcticNet (a Network of Centers of Excellence Canada) and the Natural Sciences and Engineering Research Council of Canada (NSERC) through Discovery and Northern Supplement grants to J.-C. Montero-Serrano and G. St-Onge. Finally, thanks to Gwenaëlle Chaillou (ISMER-UQAR) and France Lagroix (IPGP) for their insightful comments on an earlier version of the manuscript. Finally, the authors thank Stefanie Brachfeld (Montclair State University) and two anonymous reviewers for their constructive reviews, which improved the quality of the manuscript, as well as to B. Williams and C. Micucci for their editorial work.

## References

- Aagaard, K., & Carmack, E. C. (1989). The role of sea ice and other fresh water in the Arctic circulation. *Journal of Geophysical Research*, 94(C10), 14485–14498. <https://doi.org/10.1029/jc094ic10p14485>
- Aagaard, K., & Carmack, E. C. (1994). The Arctic Ocean and climate: A perspective. In O. M. Johannessen, R. D. Muench, & J. E. Overland (Eds.), *The polar oceans and their role in shaping the global environment* (Vol. 85, pp. 5–20). AGU.
- Agnew, T., & Silas, A. (1995). Spring seasonal climate variability in the central Canadian Arctic Islands. *Annals of Glaciology*, 21, 330–336. <https://doi.org/10.1017/s0260305500016025>
- Aitchison, J. (1986). *Monographs on statistics and applied probability*. CRC Press.
- Aitchison, J. (1990). Relative variation diagrams for describing patterns of compositional variability. *Mathematical Geology*, 22(4), 487–511. <https://doi.org/10.1007/bf00890330>
- Alkire, M. B., Jacobson, A. D., Lehn, G. O., Macdonald, R. W., & Rossi, M. W. (2017). On the geochemical heterogeneity of rivers draining into the straits and channels of the Canadian Arctic Archipelago. *Journal of Geophysical Research: Biogeosciences*, 122(10), 2527–2547. <https://doi.org/10.1002/2016jg003723>
- Appleby, P. G., & Oldfield, F. (1983). The assessment of <sup>210</sup>Pb data from sites with varying sediment accumulation rates. *Hydrobiologia*, 103(1), 29–35. <https://doi.org/10.1007/bf00028424>
- Aziz, O. I. A., & Burn, D. H. (2006). Trends and variability in the hydrological regime of the Mackenzie River basin. *Journal of Hydrology*, 319(1–4), 282–294. <https://doi.org/10.1016/j.jhydrol.2005.06.039>
- Barber, D., & Hanesiak, J. (2004). Meteorological forcing of sea ice concentrations in the southern Beaufort Sea over the period 1979 to 2000. *Journal of Geophysical Research*, 109, C06014. <https://doi.org/10.1029/2003JC002027>
- Belliveau, K. D. (2007). *Coastal geomorphology of southwest Banks Island, NWT: Historical and recent shoreline changes and implications for the future (Doctoral dissertation)*. Memorial University of Newfoundland.
- Belt, S. T., Vare, L. L., Massé, G., Manners, H. R., Price, J. C., MacLachlan, S. E., & Schmidt, S. (2010). Striking similarities in temporal changes to spring sea ice occurrence across the central Canadian Arctic Archipelago over the last 7000 years. *Quaternary Science Reviews*, 29(25–26), 3489–3504. <https://doi.org/10.1016/j.quascirev.2010.06.041>
- Bintanja, R., & Selten, F. M. (2014). Future increases in Arctic precipitation linked to local evaporation and sea-ice retreat. *Nature*, 509(7501), 479–482. <https://doi.org/10.1038/nature13259>
- Bischof, J., Clark, D. L., & Vincent, J. S. (1996). Origin of ice-rafted debris: Pleistocene paleoceanography in the western Arctic Ocean. *Paleoceanography*, 11(6), 743–756. <https://doi.org/10.1029/96pa02557>
- Bischof, J. F., & Darby, D. A. (2000). Quaternary ice transport in the Canadian Arctic and extent of Late Wisconsinan Glaciation in the Queen Elizabeth Islands. *Canadian Journal of Earth Sciences*, 36(12), 2007–2022.
- Blott, S. J., & Pye, K. (2001). GRADISTAT: A grain size distribution and statistics package for the analysis of unconsolidated sediments. *Earth Surface Processes and Landforms*, 26(11), 1237–1248. <https://doi.org/10.1002/esp.261>
- Borcard, D., Gillet, F., & Legendre, P. (2011). *Numerical ecology with R*. New York, NY: Springer.
- Bradley, R. S., & Jonest, P. D. (1993). “Little Ice Age” summer temperature variations: Their nature and relevance to recent global warming trends. *The Holocene*, 3(4), 367–376. <https://doi.org/10.1177/095968369300300409>
- Bringué, M., & Rochon, A. (2012). Late Holocene paleoceanography and climate variability over the Mackenzie slope (Beaufort Sea, Canadian Arctic). *Marine Geology*, 291, 83–96. <https://doi.org/10.1016/j.margeo.2011.11.004>
- Burdige, D. J. (1993). The biogeochemistry of manganese and iron reduction in marine sediments. *Earth-Science Reviews*, 35(3), 249–284. [https://doi.org/10.1016/0012-8252\(93\)90040-e](https://doi.org/10.1016/0012-8252(93)90040-e)
- Calvert, S. E., & Pedersen, T. F. (2007). Chapter fourteen elemental proxies for palaeoclimatic and palaeoceanographic variability in marine sediments: Interpretation and application. *Developments in Marine Geology*, 1, 567–644. [https://doi.org/10.1016/s1572-5480\(07\)01019-6](https://doi.org/10.1016/s1572-5480(07)01019-6)
- Canadian Ice Service. (2019). *Latest ice conditions*. Retrieved from <https://www.canada.ca/en/environment-climate-change/services/ice-forecasts-observations/latest-conditions.html>
- Caron, M., Montero-Serrano, J.-C., St-Onge, G., & Rochon, A. (2020). Quantifying provenance and transport pathways of Holocene sediments from the northwestern Greenland margin. *Paleoceanography and Paleoclimatology*, 34. <https://doi.org/10.1029/2019PA003809>
- Caron, M., Rochon, A., Montero-Serrano, J.-C., & St-Onge, G. (2019). Evolution of sea surface conditions on the northwestern Greenland margin during the Holocene. *Journal of Quaternary Science*, 34(7), 569–580. <https://doi.org/10.1002/jqs.3146>
- Cohen, J., Screen, J. A., Furtado, J. C., Barlow, M., Whittleston, D., Coumou, D., & Jones, J. (2014). Recent Arctic amplification and extreme mid-latitude weather. *Nature Geoscience*, 7(9), 627. <https://doi.org/10.1038/ngeo2234>
- Comiso, J. C., Meier, W. N., & Gersten, R. (2017). Variability and trends in the Arctic Sea ice cover: Results from different techniques. *Journal of Geophysical Research: Oceans*, 122(8), 6883–6900. <https://doi.org/10.1002/2017jc012768>
- Couture, N. J., Irrgang, A., Pollard, W., Lantuit, H., & Fritz, M. (2018). Coastal erosion of permafrost soils along the Yukon Coastal Plain and fluxes of organic carbon to the Canadian Beaufort Sea. *Journal of Geophysical Research: Biogeosciences*, 123, 406–422. <https://doi.org/10.1002/2017JG004166>
- Croudace, I. W., Rindby, A., & Rothwell, R. G. (2006). *ITRAX: Description and evaluation of a new multi-function X-ray core scanner*. (Vol. 267(1), pp. 51–63). Geological Society, Special Publications. <https://doi.org/10.1144/gsl.sp.2006.267.01.04>
- Croudace, I. W., & Rothwell, R. G. (2015). *Micro-XRF studies of sediment cores: Applications of a non-destructive tool for the environmental sciences*. (Vol. 17). Springer.
- Darby, D. A. (2003). Sources of sediment found in sea ice from the western Arctic Ocean, new insights into processes of entrainment and drift patterns. *Journal of Geophysical Research*, 108(C8). <https://doi.org/10.1029/2002JC001350>
- Darby, D. A., Burckle, L. H., & Clark, D. L. (1974). Airborne dust on the Arctic pack ice, its composition and fallout rate. *Earth and Planetary Science Letters*, 24(2), 166–172. [https://doi.org/10.1016/0012-821x\(74\)90093-4](https://doi.org/10.1016/0012-821x(74)90093-4)
- Darby, D. A., Myers, W. B., Jakobsson, M., & Rigor, I. (2011). Modern dirty sea ice characteristics and sources: The role of anchor ice. *Journal of Geophysical Research*, 116. <https://doi.org/10.1029/2010jc006675>

- Day, R., Fuller, M., & Schmidt, V. A. (1977). Hysteresis properties of titanomagnetites: Grain-size and compositional dependence. *Physics of the Earth and Planetary Interiors*, 13(4), 260–267. [https://doi.org/10.1016/0031-9201\(77\)90108-x](https://doi.org/10.1016/0031-9201(77)90108-x)
- Dearing, J. (1999). *Environmental magnetic susceptibility. Using the Bartington MS2 system*. Kenilworth, Chi.
- Déry, S. J., Stadnyk, T. A., MacDonald, M. K., & Gaudi-Sharma, B. (2016). Recent trends and variability in river discharge across northern Canada. *Hydrology and Earth System Sciences*, 20(12), 4801–4818. <https://doi.org/10.5194/hess-20-4801-2016>
- Deschamps, C.-E., Montero-serrano, J.-C., & St-Onge, G. (2018). Sediment provenance changes in the western Arctic Ocean in response to ice-rafting, sea-level and oceanic circulation variations since the last deglaciation. *Geochemistry, Geophysics, Geosystems*, 19(7), 2147–2165. <https://doi.org/10.1029/2017GC007411>
- Deschamps, C.-E., St-Onge, G., Montero-Serrano, J.-C., & Polyak, L. (2018). Chronostratigraphy and spatial distribution of the Chukchi and Beaufort Sea's magnetic sediments since the last deglaciation. *Boreas*, 47, 544–564. <https://doi.org/10.1111/bor.12296>
- Dickson, R., Rudels, B., Dye, S., Karcher, M., Meincke, J., & Yashayaev, I. (2007). Current estimates of freshwater flux through Arctic and subarctic seas. *Progress in Oceanography*, 73(3–4), 210–230. <https://doi.org/10.1016/j.pocean.2006.12.003>
- Dunlop, D. J. (2002). Theory and application of the day plot ( $M_{is}/M_s$  versus  $H_{cr}/H_c$ ). 1. Theoretical curves and tests using titanomagnetite data. *Journal of Geophysical Research*, 107. <https://doi.org/10.1029/2001jb000486>
- Durantou, L., Rochon, A., Ledu, D., Massé, G., Schmidt, S., & Babin, M. (2012). Quantitative reconstruction of sea-surface conditions over the last ~150 yr in the Beaufort Sea based on dinoflagellate cyst assemblages: The role of large-scale atmospheric circulation patterns. *Biogeosciences*, 9(12).
- England, J., Atkinson, N., Bednarski, J., Dyke, A. S., Hodgson, D. A., & Cofaigh Ó, C. (2006). The innuitian ice sheet: Configuration, dynamics and chronology. *Quaternary Science Reviews*, 25(7–8), 689–703. <https://doi.org/10.1016/j.quascirev.2005.08.007>
- Gajewski, K. (2002). Modern pollen assemblages in lake sediments from the Canadian Arctic. *Arctic Antarctic and Alpine Research*, 34(1), 26–32. <https://doi.org/10.1080/15230430.2002.12003465>
- Gajewski, K. (2006). Essai: Is Arctic palynology a “Blunt Instrument”? *Géographie Physique et Quaternaire*, 60(2), 95–102.
- Gajewski, K. (2015). Quantitative reconstruction of Holocene temperatures across the Canadian Arctic and Greenland. *Global and Planetary Change*, 128, 14–23. <https://doi.org/10.1016/j.gloplacha.2015.02.003>
- Gajewski, K., & Frappier, M. (2001). A Holocene lacustrine record of environmental change in northeastern Prince of Wales Island, Nunavut, Canada. *Boreas*, 30(4), 285–289.
- Gajewski, K., Garneau, M., & Bourgeois, J. C. (1995). Paleoenvironments of the Canadian High Arctic derived from pollen and plant macrofossils: Problems and potentials. *Quaternary Science Reviews*, 14(6), 609–629. [https://doi.org/10.1016/0277-3791\(95\)00015-h](https://doi.org/10.1016/0277-3791(95)00015-h)
- Gamboa, A., Montero-Serrano, J. C., St-Onge, G., Rochon, A., & Desiège, P. A. (2017). Mineralogical, geochemical, and magnetic signatures of surface sediments from the Canadian Beaufort Shelf and Amundsen Gulf (Canadian Arctic). *Geochemistry, Geophysics, Geosystems*, 18(2), 488–512. <https://doi.org/10.1002/2016gc006477>
- Ghaleb, B. (2009). Overview of the methods for the measurement and interpretation of short-lived radioisotopes and their limits. In *IOP Conference Series: Earth and environmental science* (Vol. 5, No. 1, p. 012007). IOP Publishing.
- Goñi, M. A., O'Connor, A. E., Kuzyk, Z. Z., Yunker, M. B., Gobeil, C., & Macdonald, R. W. (2013). Distribution and sources of organic matter in surface marine sediments across the North American Arctic margin. *Journal of Geophysical Research: Oceans*, 118, 4017–4035. <https://doi.org/10.1002/jgrc.20286>
- Goñi, M. A., Yunker, M. B., Macdonald, R. W., & Eglinton, T. I. (2005). The supply and preservation of ancient and modern components of organic carbon in the Canadian Beaufort Shelf of the Arctic Ocean. *Marine Chemistry*, 93(1), 53–73. <https://doi.org/10.1016/j.marchem.2004.08.001>
- Guo, L., Ping, C.-L., & Macdonald, R. W. (2007). Mobilization pathways of organic carbon from permafrost to arctic rivers in a changing climate. *Geophysical Research Letters*, 34, L13603. <https://doi.org/10.1029/2007GL030689>
- Hamilton, T. F., & Smith, J. D. (1986). Improved alpha energy resolution for the determination of polonium isotopes by alpha-spectrometry. *International Journal of Radiation Applications and Instrumentation. Part A. Applied Radiation and Isotopes*, 37(7), 628–630. [https://doi.org/10.1016/0883-2889\(86\)90084-5](https://doi.org/10.1016/0883-2889(86)90084-5)
- Hanna, A. J., Shanahan, T. M., Allison, M. A., Bianchi, T. S., & Schreiner, K. M. (2018). A multi-proxy investigation of late-Holocene temperature change and climate-driven fluctuations in sediment sourcing: Simpson Lagoon, Alaska. *The Holocene*, 28(6), 984–997. <https://doi.org/10.1177/0959683617752845>
- Hannah, C. G., Dupont, F., & Dunphy, M. (2009). Polynyas and tidal currents in the Canadian Arctic Archipelago. *Arctic*, 83–95.
- Harrison, J. C., Brent, T. A., & Oakey, G. N. (2011). Baffin Fan and its inverted rift system of Arctic eastern Canada: Stratigraphy, tectonics and petroleum resource potential. *Geological Society, London, Memoirs*, 35(1), 595–626. <https://doi.org/10.1144/m35.40>
- Helama, S., & Lindholm, M. (2003). Droughts and rainfall in south-eastern Finland since AD 874, inferred from Scots pine ring-widths. *Boreal Environment Research*, 8(2), 171–183.
- Hill, P. R., Blasco, S. M., Harper, J. R., & Fissel, D. B. (1991). Sedimentation on the Canadian Beaufort Shelf. *Continental Shelf Research*, 11(8–10), 821–842. [https://doi.org/10.1016/0278-4343\(91\)90081-g](https://doi.org/10.1016/0278-4343(91)90081-g)
- Hill, P. R., Lewis, C. P., Desmarais, S., Kauppaymuthoo, V., & Rais, H. (2001). The Mackenzie Delta: Sedimentary processes and facies of a high-latitude, fine-grained delta. *Sedimentology*, 48(5), 1047–1078. <https://doi.org/10.1046/j.1365-3091.2001.00408.x>
- Holland, M. M., & Bitz, C. M. (2003). Polar amplification of climate change in coupled models. *Climate Dynamics*, 21(3–4), 221–232. <https://doi.org/10.1007/s00382-003-0332-6>
- Howell, S. E., & Brady, M. (2019). The dynamic response of sea ice to warming in the Canadian Arctic Archipelago. *Geophysical Research Letters*, 46(22), 13119–13125. <https://doi.org/10.1029/2019gl085116>
- Huntington, T. G. (2006). Evidence for intensification of the global water cycle: Review and synthesis. *Journal of Hydrology*, 319(1), 83–95. <https://doi.org/10.1016/j.jhydrol.2005.07.003>
- Ingram, R. G., & Prinsenberg, S. (1998). Coastal oceanography of Hudson Bay and surrounding eastern Canadian Arctic waters. *The sea*, 11(29), 835–859.
- Jakobsson, M. (2002). Hypsometry and volume of the Arctic Ocean and its constituent seas. *Geochemistry, Geophysics, Geosystems*, 3(5), 1–18. <https://doi.org/10.1029/2001gc000302>
- Jones, E. P., Swift, J. H., Anderson, L. G., Lipizer, M., Civitarese, G., Falkner, K. K., & McLaughlin, F. (2003). Tracing Pacific water in the North Atlantic Ocean. *Journal of Geophysical Research*, 108. <https://doi.org/10.1029/2001jc001141>
- Jones, P. D., & Mann, M. E. (2004). Climate over past millennia. *Reviews of Geophysics*, 42(2), RG2002. <https://doi.org/10.1029/2003RG000143>
- Kassambara, A. (2016). *ggcorrplot: Visualization of a correlation matrix using “ggplot2”*. R package version 0.1.3. Retrieved from <https://cran.r-project.org/web/packages/ggcorrplot/>
- Kassambara, A. (2017). Practical guide to cluster analysis in R: Unsupervised machine learning (Vol. 1). STHDA.



- Kassambara, A., & Mundt, F. (2020). *Factoextra: Extract and visualize the results of multivariate data analyses. R package version 1.0.7*. Retrieved from <https://cran.r-project.org/web/packages/factoextra/>
- Kaufman, D. S., Ager, T. A., Anderson, N. J., Anderson, P. M., Andrews, J. T., Bartlein, P. T., et al. (2004). Holocene thermal maximum in the western Arctic 0–180°W. *Quaternary Science Reviews*, 23(18–19), 2059–2060.
- Kobayashi, D., Yamamoto, M., Irino, T., Nam, S.-I., Park, Y.-H., Harada, N., et al. (2016). Distribution of detrital minerals and sediment color in western Arctic Ocean and northern Bering Sea sediments: Changes in the provenance of western Arctic Ocean sediments since the last glacial period. *Polar Science*, 10, 519–531. <https://doi.org/10.1016/j.polar.2016.07.005>
- Koerner, R. M. (1977). Devon Island ice cap: Core stratigraphy and paleoclimate. *Science*, 196(4285), 15–18. <https://doi.org/10.1126/science.196.4285.15>
- Koerner, R. M., & Fisher, D. A. (1990). A record of Holocene summer climate from a Canadian high-Arctic ice core. *Nature*, 343(6259), 630. <https://doi.org/10.1038/343630a0>
- Koerner, R. M., & Paterson, W. S. B. (1974). Analysis of a core through the Meighen Ice Cap, Arctic Canada, and its paleoclimatic implications. *Quaternary Research*, 4(3), 253–263. [https://doi.org/10.1016/0033-5894\(74\)90015-5](https://doi.org/10.1016/0033-5894(74)90015-5)
- Kopec, B. G., Feng, X., Michel, F. A., & Posmentier, E. S. (2016). Influence of sea ice on Arctic precipitation. *Proceedings of the National Academy of Sciences*, 113(1), 46–51. <https://doi.org/10.1073/pnas.1504633113>
- Kutos, O., Rochon, A., & Montero-Serrano, J.-C. (2021). Evolution of palaeo-sea-surface conditions and sediment dynamics over the last 2700 years on the Mackenzie Slope, Beaufort Sea (Canadian Arctic). *Boreas*, 50, 893–914. <https://doi.org/10.1111/bor.12513>
- Kuzyk, Z. A., Gobeil, C., & Macdonald, R. W. (2013). <sup>210</sup>Pb and <sup>137</sup>Cs in margin sediments of the Arctic Ocean: Controls on boundary scavenging. *Global Biogeochemical Cycles*, 27, 422–439. <https://doi.org/10.1002/gbc.20041>
- Lamb, A. L., Wilson, G. P., & Leng, M. J. (2006). A review of coastal palaeoclimate and relative sea-level reconstructions using  $\delta^{13}\text{C}$  and C/N ratios in organic material. *Earth-Science Reviews*, 75, 29–57. <https://doi.org/10.1016/j.earscirev.2005.10.003>
- Lammers, R. B., Shiklomanov, A. I., Vörösmarty, C. J., Fekete, B. M., & Peterson, B. J. (2001). Assessment of contemporary Arctic river runoff based on observational discharge records. *Journal of Geophysical Research: Atmosphere*, 106(D4), 3321–3334. <https://doi.org/10.1029/2000jd900444>
- Ledu, D., Rochon, A., de Vernal, A., Barletta, F., & St-Onge, G. (2010). Holocene sea ice history and climate variability along the main axis of the Northwest Passage, Canadian Arctic. *Paleoceanography and Paleoclimatology*, 25(2).
- Ledu, D., Rochon, A., de Vernal, A., & St-Onge, G. (2010). “Holocene paleoceanography of the northwest passage, Canadian Arctic Archipelago”. *Quaternary Science Reviews*, 29, 3468–3488. <https://doi.org/10.1016/j.quascirev.2010.06.018>
- Lewkowicz, A. G., & Way, R. G. (2019). Extremes of summer climate trigger thousands of thermokarst landslides in a High Arctic environment. *Nature Communications*, 10, 1329. <https://doi.org/10.1038/s41467-019-09314-7>
- Li, G., Piper, D. J., & Calvin Campbell, D. (2011). The Quaternary Lancaster sound trough-mouth fan, NW Baffin Bay. *Journal of Quaternary Science*, 26(5), 511–522. <https://doi.org/10.1002/jqs.1479>
- Lin, P., Pickart, R. S., Fissel, D., Ross, E., Kasper, J., Bahr, F., & Wiese, F. K. (2020). Circulation in the vicinity of Mackenzie Canyon from a year-long mooring array. *Progress in Oceanography*, 187, 102396.
- Linderholm, H. W., & Chen, D. (2005). Central Scandinavian winter precipitation variability during the past five centuries reconstructed from *Pinus sylvestris* tree rings. *Boreas*, 34(1), 43–52. <https://doi.org/10.1080/03009480510012845>
- Linderholm, H. W., Nicolle, M., Francus, P., Gajewski, K., Helama, S., Korhola, A., & Debret, M. (2018). Arctic hydroclimate variability during the last 2000 years. *Climate of the Past*.
- Ljungqvist, F. C., Krusic, P. J., Sundqvist, H. S., Zorita, E., Brattström, G., & Frank, D. (2016). Northern Hemisphere hydroclimate variability over the past twelve centuries. *Nature*, 532(7597), 94. <https://doi.org/10.1038/nature17418>
- Macdonald, R. W., & Gobeil, C. (2012). Manganese sources and sinks in the Arctic Ocean with reference to periodic enrichments in basin sediments. *Aquatic Geochemistry*, 18(6), 565–591. <https://doi.org/10.1007/s10498-011-9149-9>
- Macdonald, R. W., Solomon, S. M., Cranston, R. E., Welch, H. E., Yunker, M. B., & Gobeil, C. (1998). A sediment and organic carbon budget for the Canadian Beaufort Shelf. *Marine Geology*, 144(4), 255–273. [https://doi.org/10.1016/s0025-3227\(97\)00106-0](https://doi.org/10.1016/s0025-3227(97)00106-0)
- MacLean, B., Williams, G. L., Srivastava, S. P., & Keen, M. J. (1990). Geology of Baffin Bay and Davis Strait. *Geology of Canada*, 2, 293–348.
- Maechler, M., Rousseeuw, P., Struyf, A., Hubert, M., & Hornik, K. (2019). *Cluster: Cluster analysis basics and extensions. R package version 2.1.0*. Retrieved from <https://cran.r-project.org/web/packages/cluster/>
- Magen, C., Chaillou, G., Crowe, S. A., Mucci, A., Sundby, B., Gao, A., & Sasaki, H. (2010). Origin and fate of particulate organic matter in the southern Beaufort Sea-Amundsen Gulf region, Canadian Arctic. *Estuarine, Coastal and Shelf Science*, 86(1), 31–41. <https://doi.org/10.1016/j.ecss.2009.09.009>
- Mann, M. E., Zhang, Z., Hughes, M. K., Bradley, R. S., Miller, S. K., Rutherford, S., & Ni, F. (2008). Proxy-based reconstructions of hemispheric and global surface temperature variations over the past two millennia. *Proceedings of the National Academy of Sciences*, 105(36), 13252–13257. <https://doi.org/10.1073/pnas.0805721105>
- Martens, J., Romankevich, E., Semiletov, I., Wild, B., van Dongen, B., Vonk, J., et al. (2020). CASCADE—The circum-arctic sediment carbon database. *Earth System Science Data*, 13(6), 2561–2572. <https://doi.org/10.5194/essd-2020-401>
- Mclaughlin, F., Carmack, E., Ingram, R., Williams, W., & Michel, C. (2004). Oceanography of the northwest passage. *The Sea*, 14, 1213–1244.
- Melling, H. (2002). Sea ice of the northern Canadian Arctic Archipelago. *Journal of Geophysical Research*, 107. <https://doi.org/10.1029/2001jc001102>
- Melling, H., Gratton, Y., & Ingram, G. (2001). Ocean circulation within the North Water polynya of Baffin Bay. *Atmosphere-Ocean*, 39(3), 301–325. <https://doi.org/10.1080/07055900.2001.9649683>
- Meyers, P. A. (1994). Preservation of elemental and isotopic source identification of sedimentary organic matter. *Chemical Geology*, 114(3–4), 289–302. [https://doi.org/10.1016/0009-2541\(94\)90059-0](https://doi.org/10.1016/0009-2541(94)90059-0)
- Meyers, P. A. (1997). Organic geochemical proxies of paleoceanographic, paleolimnologic, and paleoclimatic processes. *Organic Geochemistry*, 27(5–6), 213–250. [https://doi.org/10.1016/s0146-6380\(97\)00049-1](https://doi.org/10.1016/s0146-6380(97)00049-1)
- Michel, C., Ingram, R. G., & Harris, L. R. (2006). Variability in oceanographic and ecological processes in the Canadian Arctic Archipelago. *Progress in Oceanography*, 71(2–4), 379–401. <https://doi.org/10.1016/j.poccean.2006.09.006>
- Millot, R., Gaillardet, J., Dupré, B., & Allègre, C. J. (2003). Northern latitude chemical weathering rates: Clues from the Mackenzie River basin, Canada. *Geochimica et Cosmochimica Acta*, 67(7), 1305–1329. [https://doi.org/10.1016/s0016-7037\(02\)01207-3](https://doi.org/10.1016/s0016-7037(02)01207-3)
- Montero-Serrano, J. C., Palarea-Albaladejo, J., Martín-Fernández, J. A., Martínez-Santana, M., & Gutiérrez-Martín, J. V. (2010). Sedimentary chemofacies characterization by means of multivariate analysis. *Sedimentary Geology*, 228(3–4), 218–228. <https://doi.org/10.1016/j.sedgeo.2010.04.013>

- Montero-Serrano, J. C., Rioux, P., & Aebischer, S. (2016). Natural climate and oceanographic variability in the western Canadian Arctic Ocean since the last deglaciation. *ArcticNet Leg 3a Cruise Report—CCGS Amundsen*. U.S. Geological Survey.
- Mosley-Thompson, E., McConnell, J. R., Bales, R. C., Li, Z., Lin, P. N., Steffen, K., & Bathke, D. (2001). Local to regional-scale variability of annual net accumulation on the Greenland ice sheet from PARCA cores. *Journal of Geophysical Research*, *106*(D24), 33839–33851. <https://doi.org/10.1029/2001jd900067>
- Nizou, J., Hanebuth, T. J., & Vogt, C. (2011). Deciphering signals of late Holocene fluvial and aeolian supply from a shelf sediment depocentre off Senegal (north-west Africa). *Journal of Quaternary Science*, *26*(4), 411–421. <https://doi.org/10.1002/jqs.1467>
- O'Brien, M. C., Macdonald, R. W., Melling, H., & Iseki, K. (2006). Particle fluxes and geochemistry on the Canadian Beaufort Shelf: Implications for sediment transport and deposition. *Continental Shelf Research*, *26*(1), 41–81.
- Oldfield, F., & Appleby, P. G. (1984). Empirical testing of  $^{210}\text{Pb}$ -dating models for lake sediments. In *Lake sediments and environmental history*.
- Overduin, P. P., Strzelecki, M. C., Grigoriev, M. N., Couture, N., Lantuit, H., St-Hilaire-Gravel, D., & Wetterich, S. (2014). Coastal changes in the Arctic. *Geological Society, London, Special Publications*, *388*, 103–129. <https://doi.org/10.1144/sp388.13>
- Özdemir, Ö., & Dunlop, D. J. (1997). Effect of crystal defects and internal stress on the domain structure and magnetic properties of magnetite. *Journal of Geophysical Research*, *102*(B9), 20211–20224. <https://doi.org/10.1029/97jb01779>
- Pachauri, R. K., Allen, M. R., Barros, V. R., Broome, J., Cramer, W., Christ, R., & Dubash, N. K. (2014). *Climate change 2014: Synthesis report. Contribution of Working Groups I, II and III to the fifth assessment report of the Intergovernmental Panel on Climate Change*. IPCC.
- Paterson, W. S. B., & Waddington, E. D. (1984). Past accumulation rates at camp century and Devon Island, deduced from ice-core measurements. *Annals of Glaciology*, *5*, 222–223. <https://doi.org/10.1017/s026030550000392x>
- Peros, M. C., & Gajewski, K. (2008). Holocene climate and vegetation change on Victoria Island, western Canadian Arctic. *Quaternary Science Reviews*, *27*(3–4), 235–249. <https://doi.org/10.1016/j.quascirev.2007.09.002>
- Peterson, B. J., McClelland, J., Curry, R., Holmes, R. M., Walsh, J. E., & Aagaard, K. (2006). Trajectory shifts in the Arctic and subarctic freshwater cycle. *Science*, *313*(5790), 1061–1066. <https://doi.org/10.1126/science.1122593>
- Pieńkowski, A. J., England, J. H., Furze, M. F., Blasco, S., Mudie, P. J., & MacLean, B. (2013). 11,000 yrs of environmental change in the Northwest Passage: A multiproxy core record from central Parry Channel, Canadian High Arctic. *Marine Geology*, *341*, 68–85.
- Pieńkowski, A. J., Gill, N. K., Furze, M. F., Mugo, S. M., Marret, F., & Perreux, A. (2017). Arctic sea-ice proxies: Comparisons between biogeochemical and micropalaeontological reconstructions in a sediment archive from Arctic Canada. *The Holocene*, *27*(5), 665–682.
- Pieńkowski, A. J., Mudie, P. J., England, J. H., Smith, J. N., & Furze, M. F. (2011). Late Holocene environmental conditions in Coronation Gulf, southwestern Canadian Arctic Archipelago: Evidence from dinoflagellate cysts, other non-pollen palynomorphs, and pollen. *Journal of Quaternary Science*, *26*(8), 839–853.
- Pisarcic, M. F., St-Onge, S. M., & Kokelj, S. V. (2009). Tree-ring reconstruction of early-growing season precipitation from Yellowknife, Northwest Territories, Canada. *Arctic Antarctic and Alpine Research*, *41*(4), 486–496. <https://doi.org/10.1657/1938-4246-41.4.486>
- Proshutinsky, A., Bourke, R. H., & McLaughlin, F. A. (2002). The role of the Beaufort Gyre in Arctic climate variability: Seasonal to decadal climate scales. *Geophysical Research Letters*, *29*(23), 15–21. <https://doi.org/10.1029/2002gl015847>
- R Core Team. (2021). *R: A language and environment for statistical computing*. R Foundation for statistical computing. Vienna. Retrieved from <https://www.R-project.org/>
- Reimnitz, E., & Barnes, P. W. (1987). Sea-ice influence on Arctic coastal retreat. In *Coastal Sediments' 87. Proceedings of a Specialty Conference on Advances in Understanding of Coastal Sediment Processes* (Vol. 2, pp. 1578–1591).
- Reimnitz, E., Barnes, P. W., & Harper, J. R. (1990). A review of beach nourishment from ice transport of shoreface materials, Beaufort Sea, Alaska. *Journal of Coastal Research*, 439–469.
- Reimnitz, E., Clayton, J. R., Kempema, E. W., Payne, J. R., & Weber, W. S. (1993). Interaction of rising frazil with suspended particles: Tank experiments with applications to nature. *Cold Regions Science and Technology*, *21*(2), 117–135. [https://doi.org/10.1016/0165-232x\(93\)90002-p](https://doi.org/10.1016/0165-232x(93)90002-p)
- Reimnitz, E., & Maurer, D. K. (1979). Effects of storm surges on the Beaufort Sea coast, northern Alaska. *Arctic*, 329–344.
- Richerol, T., Rochon, A., Blasco, S., Scott, D. B., Schell, T. M., & Bennett, R. J. (2008). Evolution of paleo sea-surface conditions over the last 600 years in the Mackenzie Trough, Beaufort Sea (Canada). *Marine Micropaleontology*, *68*(1–2), 6–20. <https://doi.org/10.1016/j.marmicro.2008.03.003>
- Ruppel, M., Väiliranta, M., Virtanen, T., & Korhola, A. (2013). Postglacial spatiotemporal peatland initiation and lateral expansion dynamics in North America and northern Europe. *The Holocene*, *23*(11), 1596–1606. <https://doi.org/10.1177/0959683613499053>
- Schell, T. M., Moss, T. J., Scott, D. B., & Rochon, A. (2008). Paleo-sea ice conditions of the Amundsen Gulf, Canadian Arctic Archipelago: Implications for the foraminiferal record of the last 200 years. *Journal of Geophysical Research: Oceans*, *113*. <https://doi.org/10.1029/2007JC004202>
- Schlitzer, R. (2018). *Ocean data view*. Retrieved from <https://odv.awi.de>
- Scott, D. B., Schell, T., St-Onge, G., Rochon, A., & Blasco, S. (2009). Foraminiferal assemblage changes over the last 15,000 years on the Mackenzie-Beaufort Sea Slope and Amundsen Gulf, Canada: Implications for past sea ice conditions. *Paleoceanography*, *24*. <https://doi.org/10.1029/2007pa001575>
- Serreze, M. C., Barrett, A. P., Stroeve, J. C., Kindig, D. N., & Holland, M. M. (2008). The emergence of surface-based Arctic amplification. *The Cryosphere Discussions*, *2*(4), 601–622.
- Serreze, M. C., & Francis, J. A. (2006). The Arctic amplification debate. *Climatic Change*, *76*(3–4), 241–264. <https://doi.org/10.1007/s10584-005-9017-y>
- Serreze, M. C., & Stroeve, J. (2015). Arctic sea ice trends, variability and implications for seasonal ice forecasting. *Philosophical Transactions of the Royal Society A: Mathematical, Physical and Engineering Sciences*, *373*(2045), 20140159.
- Steffen, K. (1986). Ice conditions of an Arctic polynya: North Water in winter. *Journal of Glaciology*, *32*(112), 383–390.
- St-Hilaire-Gravel, D., Forbes, D. L., & Bell, T. (2011). Multitemporal analysis of a gravel-dominated coastline in the central Canadian Arctic Archipelago. *Journal of Coastal Research*, *28*(2), 421–441.
- Stokes, C. R., Clark, C. D., Darby, D. A., & Hodgson, D. A. (2005). Late Pleistocene ice export events into the Arctic Ocean from the M'Clure Strait ice stream, Canadian Arctic Archipelago. *Global and Planetary Change*, *49*(3–4), 139–162. <https://doi.org/10.1016/j.gloplacha.2005.06.001>
- Stokes, C. R., Clark, C. D., & Storrar, R. (2009). Major changes in ice stream dynamics during deglaciation of the north-western margin of the Laurentide Ice Sheet. *Quaternary Science Reviews*, *28*(7–8), 721–738. <https://doi.org/10.1016/j.quascirev.2008.07.019>
- Stoner, J. S., & St-Onge, G. (2007). Chapter three magnetic stratigraphy in paleoceanography: Reversals, excursions, paleointensity, and secular variation. *Developments in Marine Geology*, *1*, 99–138. [https://doi.org/10.1016/s1572-5480\(07\)01008-1](https://doi.org/10.1016/s1572-5480(07)01008-1)

- St-Onge, G., & Hillaire-Marcel, C. (2001). Isotopic constraints of sedimentary inputs and organic carbon burial rates in the Saguenay Fjord, Quebec. *Marine Geology*, *176*(1–4), 1–22. [https://doi.org/10.1016/s0025-3227\(01\)00150-5](https://doi.org/10.1016/s0025-3227(01)00150-5)
- Stroeve, J. C., Maslanik, J., Serreze, M. C., Rigor, I., Meier, W., & Fowler, C. (2011). Sea ice response to an extreme negative phase of the Arctic Oscillation during winter 2009/2010. *Geophysical Research Letters*, *38*. <https://doi.org/10.1029/2010gl045662>
- van den Boogaart, K. G., & Tolosana-Delgado, R. (2008). Compositions: A unified R package to analyze compositional data. *Computers & Geosciences*, *34*, 320–338. <https://doi.org/10.1016/j.cageo.2006.11.017>
- van den Boogaart, K. G., & Tolosana-Delgado, R. (2013). *Analyzing compositional data with R*. Springer-Verlag.
- van den Boogaart, K. G., & Tolosana-Delgado, R. (2021). *Compositions: Compositional data analysis. R package version 2.0.1*. Retrieved from <https://cran.r-project.org/web/packages/compositions/>
- Vare, L. L., Masse, G., Gregory, T. R., Smart, C. W., & Belt, S. T. (2009). Sea ice variations in the central Canadian Arctic Archipelago during the Holocene. *Quaternary Science Reviews*, *28*(13–14), 1354–1366. <https://doi.org/10.1016/j.quascirev.2009.01.013>
- Viau, A. E., & Gajewski, K. (2009). Reconstructing millennial-scale, regional paleoclimates of boreal Canada during the Holocene. *Journal of Climate*, *22*(2), 316–330. <https://doi.org/10.1175/2008jcli2342.1>
- Vinther, B. M., Buchardt, S. L., Clausen, H. B., Dahl-Jensen, D., Johnsen, S. J., Fisher, D. A., & Blunier, T. (2009). Holocene thinning of the Greenland ice sheet. *Nature*, *461*(7262), 385–388. <https://doi.org/10.1038/nature08355>
- von Eynatten, H., Barceló-Vidal, C., & Pawlowsky-Glahn, V. (2003). Composition and discrimination of sandstones: A statistical evaluation of different analytical methods. *Journal of Sedimentary Research*, *73*(1), 47–57. <https://doi.org/10.1306/070102730047>
- von Eynatten, H., Tolosana-Delgado, R., Karius, V., Bachmann, K., & Caracciolo, L. (2016). Sediment generation in humid Mediterranean setting: Grain-size and source-rock control on sediment geochemistry and mineralogy (Sila Massif, Calabria). *Sedimentary Geology*, *336*, 68–80. <https://doi.org/10.1016/j.sedgeo.2015.10.008>
- Wagner, A., Lohmann, G., & Prange, M. (2011). Arctic river discharge trends since 7ka BP. *Global and Planetary Change*, *79*(1), 48–60. <https://doi.org/10.1016/j.gloplacha.2011.07.006>
- Wanner, H., Solomina, O., Grosjean, M., Ritz, S. P., & Jetel, M. (2011). Structure and origin of Holocene cold events. *Quaternary Science Reviews*, *30*(21–22), 3109–3123. <https://doi.org/10.1016/j.quascirev.2011.07.010>
- Wheeler, J. O., Hoffman, P. F., Card, K. D., Davidson, A., Sanford, B. V., Okulitch, A. V., & Roest, W. R. (1996). *Geological map of Canada Natural Resources Canada*.
- Woodgate, R. A., Aagaard, K., Swift, J. H., Smethie, W. M., & Falkner, K. K. (2007). Atlantic water circulation over the Mendeleev Ridge and Chukchi Borderland from thermohaline intrusions and water mass properties. *Journal of Geophysical Research*, *112*. <https://doi.org/10.1029/2005jc003416>
- Xu, B. C., Bianchi, T. S., Allison, M. A., Dimova, N. T., Wang, H. J., Zhang, L. J., et al. (2015). Using multi-radiotracer techniques to better understand sedimentary dynamics of reworked muds in the Changjiang River estuary and inner shelf of East China Sea. *Marine Geology*, *370*, 76–86. <https://doi.org/10.1016/j.margeo.2015.10.006>
- Zabenskie, S., & Gajewski, K. (2007). Post-glacial climatic change on Boothia Peninsula, Nunavut, Canada. *Quaternary Research*, *68*(2), 261–270. <https://doi.org/10.1016/j.yqres.2007.04.003>
- Zhang, D. (2000). *Flux de radio-isotopes à courte période dans les bassins marins marginaux de l'est canadien (Doctoral dissertation, Ph. D. thesis)*. Montréal, QC: Université du Québec à Montréal.
- Zhang, H., Amesbury, M. J., Ronkainen, T., Charman, D. J., Gallego-Sala, A. V., & Väliranta, M. (2017). Testate amoeba as palaeohydrological indicators in the permafrost peatlands of north-east European Russia and Finnish Lapland. *Journal of Quaternary Science*, *32*, 976–988. <https://doi.org/10.1002/jqs.2970>
- Zhang, X., He, J., Zhang, J., Polyakov, I., Gerdes, R., Inoue, J., & Wu, P. (2013). Enhanced poleward moisture transport and amplified northern high-latitude wetting trend. *Nature Climate Change*, *3*(1), 47. <https://doi.org/10.1038/nclimate1631>